A Survey of EMI Research in Power Electronics Systems With Wide-Bandgap Semiconductor Devices

Boyi Zhang, *Student Member, IEEE*, and Shuo Wang, *Fellow, IEEE*

Abstract—Wide-bandgap (WBG) power semiconductor devices have become increasingly popular due to their superior characteristics compared to their Si counterparts. However, their fast switching speed and the ability to operate at high frequencies brought new challenges, among which the electromagnetic interference (EMI) is one of the major concerns. Many works investigated the structures of WBG power devices and their switching performance. In some cases, the conductive or radiated EMI was measured. However, the EMI-related topics, including their influence on noise sources, noise propagation paths, EMI reduction techniques, and EMC reliability issues, have not yet been systematically summarized for WBG devices. In this article, the literature on EMI research in power electronics systems with WBG devices is reviewed. Characteristics of WBG devices as EMI noise sources are reviewed. EMI propagation paths, near-field coupling, and radiated EMI are surveyed. EMI reduction techniques are categorized and reviewed. Specifically, the EMI-related reliability issues are discussed, and solutions and guidelines are presented.

Index Terms—Electromagnetic interference (EMI), gallium nitride (GaN), packaging optimization, power module, silicon carbide (SiC), wide-bandgap (WBG) devices.

I. INTRODUCTION

WITH the development of power electronics, there is an increasing demand for high-efficiency and high-power-density design. The performance of power semiconductor devices is being pushed to the limit of Si material. At the same time, wide-bandgap (WBG) semiconductor materials, including silicon carbide (SiC) and gallium nitride (GaN) [1], have presented multiple advantages over Si. As a result, WBG power devices have played an increasingly important role in power electronics systems [1]–[5]. The comparison of some properties between Si and WBG materials is shown in Table I. WBG materials present higher critical electric field, higher saturation drift velocity, higher electron mobility (GaN), and higher thermal conductivity (SiC) than Si materials. The limits of these properties, which

TABLE I
COMPARISON OF MATERIAL PROPERTIES [6]–[8]

Parameter	Si	SiC	GaN
Bandgap E_g (eV)	1.12	3.2	3.4
Critical Field E_{crit} (MV/cm)	0.3	3.5	3.3
Electron Mobility μ_n (cm^2/(V·s))	1500	650	990-2000
Permittivity ε_r	11.8	9.7	9
Thermal Conductivity (W/cm°C)	1.5	4.9	1.3
Saturation Drift Velocity (cm/s ·10^7)	1	2.7	2.7

have been the barriers to higher power density design for Si materials, have been greatly elevated by WBG materials.

With the commercialization of WBG power devices [2], it has been proven in many applications that WBG devices can achieve higher efficiency, higher power density, and higher temperature withstand ability [6]–[11] than Si devices. However, the high *dv/dt* and *di/dt* during switching transient, the voltage and current high-frequency (HF) ringing (can be up to 100 MHz) caused by parasitic inductance, as well as high operating frequency raises the concern of electromagnetic interference (EMI). Meanwhile, the high switching speed and the unique structures of WBG devices also cause power converter reliability issues. As an inevitable design consideration, EMI issues must be addressed properly; otherwise, the benefits of WBG power devices will be compromised.

Power semiconductor devices include power diodes and active power switches. Although the diodes made from the GaN material were mentioned in [2], SiC diodes are the most mature WBG diodes in industrial applications because of their relatively low material and manufacturing cost. For active power switches, the most popular ones made with WBG materials are SiC MOSFETs [9] and GaN high-electron-mobility transistors (HEMTs) [2]. As a result, in this article, the discussion focuses on SiC Schottky diodes, SiC MOSFETs, and GaN HEMTs.

In this article, the research in literature will be summarized and organized systematically. Challenges brought by WBG devices will be reviewed in detail. State-of-the-art EMI reduction techniques for the systems powered by WBG device are to be summarized. The rest of this article will be organized as follows. Section II discusses the switching characteristics of WBG power semiconductor devices.
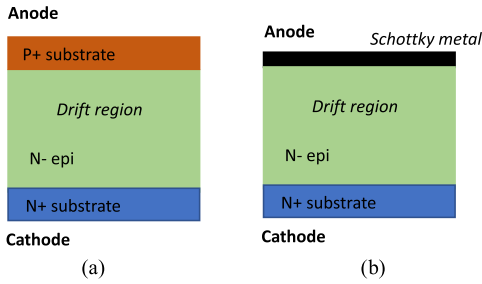
Fig. 1. Diode structure. (a) p-n junction diode. (b) Schottky diode.

The relationship between switching characteristics and EMI noise sources will be summarized. The EMI performance in power electronics systems with WBG devices will be reviewed in Section III. Both conductive and radiated EMI will be discussed. Section IV summarizes the EMI reduction techniques. Advantages and limitations of these techniques are discussed. Section V discusses the EMI-related reliability issues in power converter with WBG devices. Principles and solutions are presented. Section VI concludes this article and summarized possible future works.

II. POPULAR WBG DEVICES AND THEIR EMI CHARACTERISTICS

As shown in Table I, WBG materials have multiple superior properties to Si. As a result, the power semiconductor devices made from WBG materials can achieve lower power losses. In this section, the fundamentals of these characteristics are reviewed from an EMI perspective.

A. WBG Diodes and Their Switching Characteristics

The large concentration of free carriers in the drift region of p-n junction diode provides low ON-state voltage drop. However, to switch the diode from ON-state to voltage blocking state, these free carriers must be removed. A large reverse current will occur before the p-n junction diode can block voltage, which is known as the reverse recovery current [8]. The reverse recovery current during the diode's hard switching process causes switching power loss as well as EMI [10]. Si Schottky barrier diode (SBD) was designed to eliminate the reverse recovery currents.

Using SBDs could potentially eliminate the reverse recovery current; however, a thick lightly doped drift region, as shown in Fig. 1, must be used to block reverse voltage. Consequently, the drift region will cause a resistive forward voltage drop. To keep the ON-resistance low, the drift region of the Si Schottky diode should be very thin. As a result, the breakdown voltage becomes a limitation of Si Schottky diodes.

On the other hand, SiC material presents a huge advantage in this case. As shown in Table I, due to its high critical field, SiC SBD could have thinner drift region than Si SBDs under the same breakdown voltages. This leads to smaller resistance and lower forward voltage. The ON-resistance of a device can be calculated as follows [7]:

$$R_{ON} = \frac{4V_{BR}^2}{\varepsilon_0 \cdot \varepsilon_r \cdot \mu_n \cdot E_{crit}^3} \quad (1)$$

where V_{BR} is the breakdown voltage, ε_0 and ε_r are dielectric constant and relative permittivity of the material, respectively, μ_n is the electron mobility, and E_{crit} is the critical electric field. Based on (1), because of the critical electrical field of WBG materials, power devices made from WBG materials can have much smaller ON-resistance than those made from Si materials under the same breakdown voltages. For SiC material, the drift region resistance can be approximated as [8]

$$R_{ON}(Si) = 5.93 \times 10^{-9} V_{BR}^{2.5} \quad (2)$$
$$R_{ON}(SiC) = 2.97 \times 10^{-12} V_{BR}^{2.5}. \quad (3)$$

As shown in (2) and (3), under the same breakdown voltage requirement, the drift region for the diodes made of SiC material has nearly 2000 times smaller ON-resistance than that for the diodes made of Si material. Meanwhile, for the same ON-resistance, the SiC SBDs have much higher breakdown voltage than Si SBDs, so they are suitable for high-power applications. As a result, the SiC SBDs have become a promising replacement for Si p-n diodes.

Three different diodes were discussed in [10]. As shown in Fig. 2(a), the reverse recovery currents and reverse recovery time for the three diodes are different. SiC SBDs have the smallest reverse recovery current. The reverse recovery current of a diode determines the overshoot of its turn-on current [10], [11]. The overshoot generates EMI, so SiC SBDs are good for the reduction of EMI. The comparison of the current spectra of these three diodes is shown in Fig. 2(b). It is shown that the SiC SBD has the lowest EMI. However, as stated in [10], the benefit of EMI reduction by replacing Si diode with SiC SBD is limited. This is because the EMI performance of the whole system is not only determined by diodes but also other semiconductor switches and parasitic parameters.

B. WBG Power Switches and Their Switching Characteristics

The structures of SiC MOSFET and GaN HEMT are discussed in [2] and [9]. Because of the high critical field in Table I, the drift region of WBG power switches is usually narrower than that of their Si counterparts with the same power ratings. From (1), with an acceptable ON-resistance, the switching device made with WBG material has much smaller die size than Si devices under the same breakdown voltage requirement. With smaller die size, the junction capacitance of WBG devices is smaller than that of Si devices.

The junction capacitance of a power device can be approximately described by

$$C = \varepsilon_0 \varepsilon_r \frac{WL}{t} \quad (4)$$

where W and L are the width and length of the plate, respectively; t is the thickness between the two plates. For power devices, the gate-to-source capacitance C_{gs} is usually much bigger than the gate-to-drain capacitance C_{gd} and drain-to-source C_{ds} due to the small distance between gate and source, as shown in Table II. For WBG switches, because the die sizes are usually much smaller than Si switches [9], C_{gs} and C_{gd} of SiC MOSFET and GaN HEMT are much smaller than those of their Si counterparts. In high-voltage and
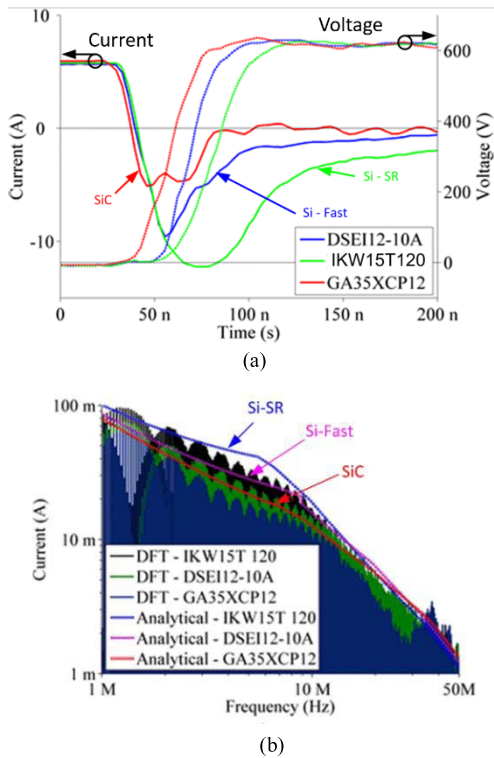
(a)

(b)

Fig. 2. Comparison of a Si p-n junction diode and a SiC SBD. (a) Current switching waveforms. (b) Current spectra [10].

TABLE II
COMPARISON OF PARASITIC CAPACITANCE OF Si IGBT, SiC MOSFET, AND GaN HEMT

Transistor	Power Rating	Input Capacitance	Output Capacitance	Reverse Transfer Capacitance
SiC MOSFET (SCT20N120)	1200 V 20A	650 pF	65 pF	14 pF
Si MOSFET (IXFX 20N120)	1200 V 20A	7400 pF	550 pF	100 pF
GaN HEMT (IGLD60R070D1)	600 V 60A	380 pF	72 pF	0.3 pF
Si MOSFET (SiHG70N60AEF)	600 V 60A	5348 pF	238 pF	7 pF

high-power applications, Si MOSFETs would have to increase the thickness of the drift region for high breakdown voltages, and at the same time, die sizes have to increase to maintain acceptable ON-resistance. As a result, the output capacitance C_{ds} of Si MOSFETs is also bigger than that of SiC MOSFETs. A similar conclusion can be applied to GaN HEMTs. C_{gs}, C_{gd}, and C_{ds} of commercial SiC MOSFET and GaN HEMT are compared with those of Si MOSFET at the same power ratings (1200 V/20 A and 600 V/60 A) and packages in Table II.

The device switching transient is discussed in detail [11]–[13]. During switching transient, the junction capacitances along with the gate resistors contribute to the time constant, which determines the switching speed of the device. With smaller junction capacitances, WBG devices are able to switch at a higher speed than Si MOSFETs. As shown in Fig. 3, the turn-on and turn-off time of GaN HEMT is 40% shorter than Si MOSFET [14].
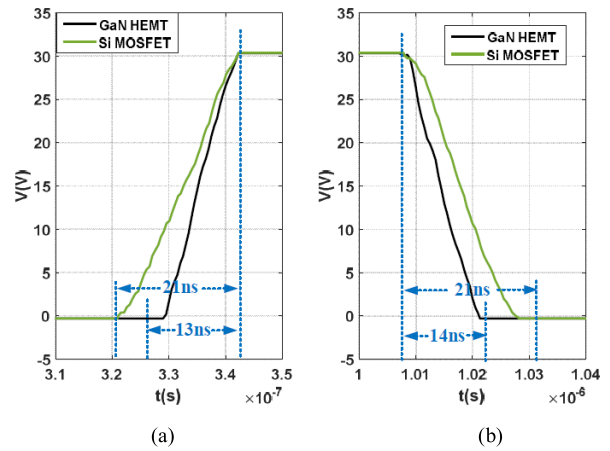

(a)   (b)

Fig. 3. Switching waveform comparison between GaN HEMT and Si MOSFET during (a) turn-off and (b) turn-on [14].

Specifically, GaN HEMTs have a unique structure. The layer between AlGaN and GaN is a high-mobility electron layer called 2-D electron gas (2DEG). The 2DEG provides a channel between drain and source. Thus, GaN HEMT is a depletion-mode (normally on) device by nature [2]. Theoretically, a normally on device can also be used as power switches, but it requires a complicated driver design.

To obtain a normally off device, several techniques, such as gate improvements [2], are proposed. For enhancement-mode GaN HEMTs, because of higher electron mobility of GaN, based on (1), the ON-resistance of GaN HEMT can be further reduced and the switching speed of GaN can be further increased. A cascode structure was proposed for a normally off GaN HEMT, where a low-power Si MOSFET is used to control a depletion-mode GaN HEMT [4]. Although it has been presented in [4] that under zero voltage switching (ZVS), cascode GaN HEMT could reduce switching power loss, and adding a low-power MOSFET will inevitably sacrifice switching speed.

In addition, because of the increased switching speed, the switching power loss of WBG devices can be reduced. As a result, WBG devices can operate at a higher frequency than Si devices [18].

Another major advantage of WBG materials is that WBG devices have the potential to operate under much higher temperatures [21]. The maximum allowed temperature of SiC and GaN can be as high as 600 °C. In comparison, the maximum allowed temperature of Si is around 150 °C–300 °C. However, the devices made from a WBG material normally have lower maximum allowed temperature limits than the material itself due to the limitation of packaging techniques. The typical maximum allowed temperature of SiC MOSFET and GaN HEMT is 150 °C–175 °C. However, it should be noted that power devices made from WBG materials have the potential to endure higher temperatures. The relationship between device core temperature and EMI characteristics has not been reported. Therefore, the core temperature discussions will not be included in this article.

In general, WBG devices have three advantages over their Si counterparts: 1) smaller reverse recovery current and reverse
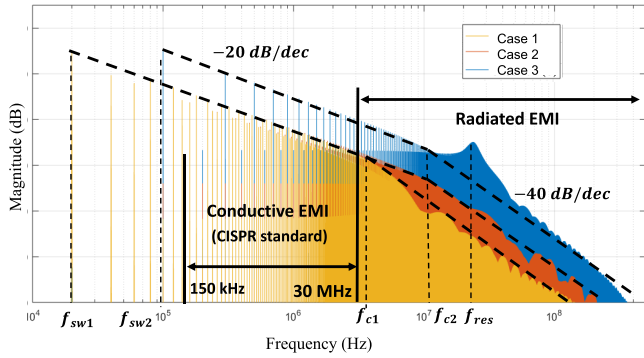
Fig. 4. Characteristic frequency spectra of the noise source voltages of a standard PWM buck converter.

recovery time; 2) faster switching speed; and 3) higher operating frequency. These three factors are good for high-efficiency and high-density design. However, from an EMI perspective, these characteristics will have a negative impact on both conductive and radiated EMIs.

C. Characteristics of WBG Devices as EMI Noise Sources

In addition to the faster switching speed and higher switching frequency, the voltage and current ringing during switching transient is more severe in WBG devices' applications than Si devices' applications [22]–[24]. The oscillation frequency can be approximately expressed as: $f_{osc} = 1/2\pi (L_{para} C_j)^{1/2}$ [24], where L_{para} is the parasitic inductance of the layout and C_j is the junction capacitance of the power device. The value of parasitic inductance is usually less than 50 nH depending on layouts, and the junction capacitances of the power devices are <1 nF, as shown in Table II. As a result, the oscillation frequency is usually higher than several megahertz, in some cases even hundreds of megahertz [14]. Therefore, the increased EMI noise would be at high frequencies (> several megahertz). HF EMI noise could be difficult to reduce because EMI filters' HF performance is limited by magnetic materials and filter's parasitic parameters [26], [27].

The influence of faster switching speed and higher switching frequency on a trapezoidal waveform has been studied in detail in [18]–[20]. In this article, a characteristic frequency spectrum of the drain-to-source voltage of a standard pulse width modulation (PWM) buck converter is presented in Fig. 4 to show how the switching characteristics of WBG device influence the EMI noise sources.

To investigate the impact of switching speed, operating frequency, and voltage ringing on the spectra of EMI noise sources individually, three cases are simulated as follows.

1) The switching frequency is f_{sw1}; the switching speed is represented by the turn-on time (t_{r1}) and turn-off time (t_{f1}); no voltage ringing.
2) The switching frequency is f_{sw1}; the switching speed is higher than situation 1): the turn-on time $t_{r2} < t_{r1}$ and turn-off time $t_{f2} < t_{f1}$; no voltage ringing.
3) The switching frequency f_{sw2} is higher than the previous two situations: $f_{sw2} > f_{sw1}$; the switching speed is the same as situation 2). In addition, a voltage ringing with the ringing frequency of f_{res} is included (in real

applications, the ringing magnitude and frequency are determined by the parasitic inductance of the package and junction capacitance of the power devices).

The duty cycle for all three situations is 0.4. Based on these situations, the influence of switching speed, switching frequency, and voltage ringing can be compared individually in Fig. 4.

As discussed in [20], the roll-off corner frequency is determined by the smaller value of turn-on and turn-off time. $f_c = 1/(\pi \cdot \min(t_r, t_f))$. Therefore, the corner frequency f_{c2} in situation 2) is higher than the corner frequency f_{c1} in situation (1). As shown in Fig. 4, the spectrum of EMI noise source in situation 2) would be higher than situation 1) after f_{c1}.

When the switching frequency is increased in situation 3), the magnitude of EMI is higher than that in situation 2) in Fig. 4 above the switching frequency. Meanwhile, the voltage ringing will result in a spike in the spectrum at the ringing frequency f_{res}.

As shown in Fig. 4, the switching frequencies and the magnitudes of the switching waveforms determine the low-frequency EMI. The switching speed and the ringing determine HF EMI.

From the earlier discussions, fast switching speed, high switching frequency, and ringing of WBG devices can all increase the spectrum of EMI noise source. Because WBG devices have higher switching speed, higher switching frequency, and higher ringing than Si devices, it can be concluded that the EMI noise generated by WBG devices would be higher than Si devices above their switching frequencies.

III. EMI PERFORMANCE COMPARISON BETWEEN Si AND WBG DEVICE APPLICATIONS

In power electronics systems, the voltage and current of power devices are EMI noise sources. The total EMI is measured with line impedance stabilization networks (LISNs) for conductive EMI and with antennas for radiated EMI. Therefore, to compare the EMI performance of WBG devices and Si devices, the characteristics of EMI noise sources and EMI propagation paths are both important. In this section, the measured EMI noise for WBG devices and Si devices is reviewed and compared in detail. The relationship between the switching characteristics and the EMI is shown. The EMI propagation paths are presented. The influence of noise sources and propagation paths on both conductive and radiated EMI is discussed.

A. Conductive EMI

The conductive EMI frequency range is different in various standards. In FCC 15 regulations, the conductive emission frequency range is from 450 kHz to 30 MHz. In CISPR22 and EN55022 standards, the frequency range is from 150 kHz to 30 MHz. In this article, the EMI from 150 kHz to 30 MHz is considered as conductive EMI.

As presented in Section II, the switching characteristics of WBG device lead to high noise spectrum magnitude. However, the measured EMI noise can be different with different power ratings and circuit topologies. Therefore, the measured
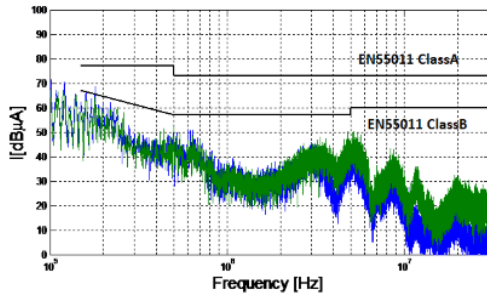
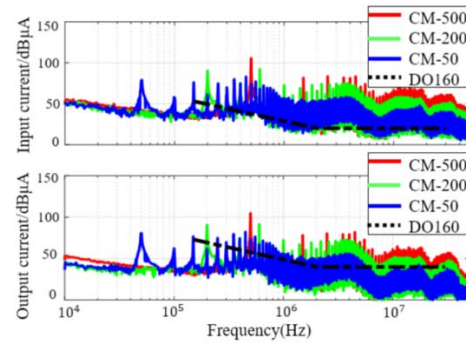Fig. 5. Measured total conductive EMI for Si IGBT and SiC MOSFET [31].

Fig. 6. Input and output CM current spectrum for a GaN-HEMT inverter switching at 50, 200, and 500 kHz [32].

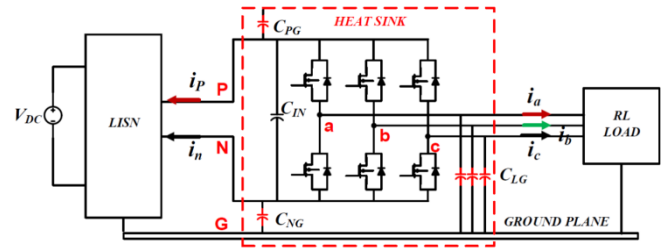Fig. 7. Three-phase inverter schematic with parasitic capacitances.

conductive EMI must be compared for WBG devices and Si devices under the same topology and power rating to evaluate the EMI performance of WBG device applications.

For low-power applications, GaN HEMTs have higher switching speed, so they usually operate at higher switching frequencies than Si MOSFETs. This leads to higher EMI at high frequencies starting from the switching frequencies of the GaN HEMTs. For high-power applications, SiC MOSFETs have higher switching speed, so they usually operate at higher switching frequencies than Si IGBTs. This leads to higher EMI at high frequencies starting from the switching frequencies of the SiC MOSFETs.

For high-power applications, although the switching frequencies are not as high as those in lower power applications, because the amplitudes of switching voltages and currents are high, the EMI is still significant. On the other hand, in low-power applications, although the switching voltages or currents could be smaller than those in high-power applications, because the switching devices usually operate at higher switching frequencies, the HF EMI could be significant.

A comparison of conductive EMI between matrix converters with Si IGBTs and SiC MOSFETs is shown in Fig. 5 [31]. Si IGBT and SiC MOSFET switch at the same frequency (10 kHz). The switching speed is 11 kV/μs for SiC MOSFETs and 6.6 kV/μs for Si IGBTs. The measured EMI noise of SiC MOSFET is 20 dB higher than that of Si IGBT from 10 to 30 MHz. In Fig. 6, the conductive EMI is measured for a 1-kW 400-V GaN HEMT inverter as shown in Fig. 7 at 50-, 200-, and 500-kHz switching frequencies. The EMI at 500-kHz switching frequency is 20 dB higher than the EMI at 50-kHz switching frequency from 500 kHz to 30 MHz. From Figs. 5 and 6, both high switching speed and high switching frequencies can increase conductive EMI. This agrees with Fig. 4. When WBG devices operate at higher speed and higher frequency than Si devices, the conductive EMI issue is the most serious. In the case of [45], the conductive EMI of a converter with GaN HEMTs (42 kV/μs and 100 kHz) is more than 30 dB higher than that with Si IGBTs (15 kV/μs and 20 kHz) from 10 to 30 MHz.

Another factor that determines the conductive EMI noise is the impedance of EMI propagation paths. The impedance of the EMI propagation path depends on the circuit topology, grounding connections, and component characteristics. A three-phase inverter schematic with parasitic capacitance and LISN is shown in Fig. 7. During operation, the voltage potentials of points a, b, and c change drastically, causing

common mode (CM) EMI noise current to flow to the ground through the parasitic capacitances. The CM current is measured through LISNs. In [35] and [36], the conductive EMI noise in motor drive application using SiC JFETs, which is similar to that in Fig. 7, is analyzed. Lemmon *et al.* [3] presented the conductive EMI analysis for an inverter without grounding in shipboard applications. As shown in Fig. 7, parasitic capacitance plays a major role in CM EMI noise paths for the three-phase topology. It was also shown in [33] that the parasitic capacitance is the major contributor of CM noise propagation path impedance for single-phase converter. The impedance of parasitic capacitance is inversely proportional to frequencies. The reduction of CM path impedance at high frequencies can further worsen the EMI issue. In [31], in an inverter, the CM EMI noise of SiC MOSFET is 10–20 dB higher from 7 to 30 MHz than that of Si IGBT.

Different from CM noise, differential mode (DM) noise circulates inside the circuits. Therefore, the DM noise propagation path is determined by circuit topology and component characteristics. Systems with WBG devices have higher HF DM spectrum (>1 MHz) than the systems with Si devices. In [31], DM noise is increased by 8 dB from 3 to 30 MHz with WBG devices. The conclusions in this section can be applied to both single- and three-phase topologies because the analysis of EMI noise sources, namely the switching waveforms of the power device, can be applied to both systems. Systematical comparisons are made and summarized in Table III. The characteristics of WBG devices and EMI consequences are listed.

B. Near-Field Emission

As mentioned in Section II, WBG devices have higher radiated EMI noise than Si devices. At the same time, in high-power-density design, components are very close to each

TABLE III
EMI Characteristic Comparison Between the Systems With Si and WBG Devices

EMI related characteristics	System with Si devices	System with WBG devices	Consequence
Switching speed	Si IGBT (>900 V/30 A): <14.23kV/us [106]	SiC MOSFET (>900 V/30 A): < 24 kV/us [18]	The systems with WBG devices have higher noise magnitude in high frequency conductive and radiated EMI noise range than the systems with Si devices.
	Si MOSFET: < 15kV/us [11]	GaN HEMT: < 65.8kV/us [82]	
Voltage oscillation	Small oscillation due to slow switching speed caused by large junction capacitance [14]	Serious oscillation due to fast switching speed caused by small junction capacitance [14]	The systems with WBG devices have higher EMI at the oscillation frequencies than the systems with Si devices.
Switching frequency	< 20kHz [31] for Si IGBT) (<1MHz for Si MOSFET)	<100kHz [32] for SiC MOSFET, <5 MHz for GaN HEMT [33])	The systems with WBG devices have higher EMI above switching frequencies than the systems with Si devices. Both conductive and radiative EMI increases with WBG devices. CM noise increases due to smaller parasitic capacitance impedance at high frequencies.

other. This raises the concern of near-field coupling. Although WBG devices have been commercialized for a while, there are a very limited number of research articles on the near-field coupling and far-field radiation in power electronics systems. Therefore, this section also includes some articles on Si devices that could be applied to WBG devices.

In this article, a distinction is made between the near field and the far field. As explained in [37], when the distance r between the radiation source and the observation point is much smaller than $\lambda/2\pi$, it is considered as near-field region, where λ is the wavelength of the electromagnetic wave. In the near-field region, the electric field and the magnetic field are determined by the voltages, currents, and the geometry of their emission sources. Either electric field or magnetic field will be dominant depending on the noise source characteristics. When the distance $r \gg \lambda/2\pi$, it is considered as far-field region. The electric field and the magnetic field are coupled via Maxwell's equations.

For the emission from the converter circuit or passive components, the distance between the observation point and the emission source is usually much smaller than $\lambda/2\pi$. As a result, it is considered as a near-field region. There are two different near-field couplings in power electronics systems: near magnetic field coupling and near electric field coupling. Near electric field coupling can be represented with parasitic capacitance. The capacitance is determined by the geometry of the physical structures, which can be calculated with analytical methods [38]. The emission sources of the near electric field are usually nodes with pulsating voltage.

As for near magnetic coupling, the emission sources are usually current loops. Three emission sources have been recognized: 1) DM current loop between paralleled devices in Fig. 8(a); 2) CM current loop between input cables and ground in Fig. 8(b); and 3) near magnetic field emitted from magnetic components in Fig. 8(c) [41], [43], [44]. The magnetic flux density can be calculated with Biot–Savart's law in [39]. However, Biot–Savart's law is difficult to calculate complicated geometry such as in Fig. 9(c). Numerical methods, such as finite-difference time-domain (FDTD) method [38], are commonly used to predict near magnetic field emission.
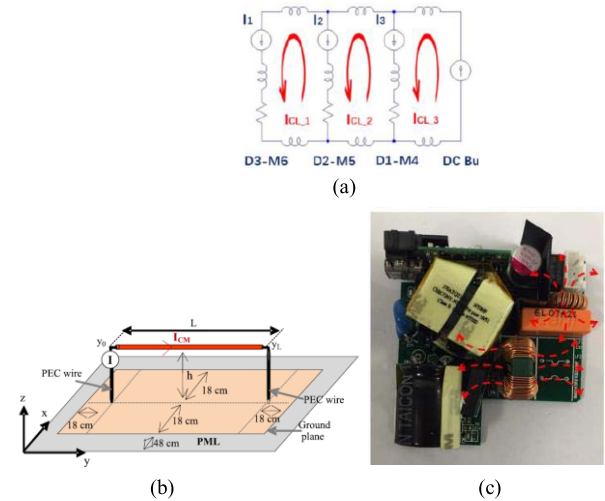

Fig. 8. Near magnetic field emission sources. (a) DM current loop [39]. (b) CM current loops between cables and ground [40]. (c) Leakage magnetic flux (red dash arrows) of magnetic components [41].

As analyzed in Section III-A, WBG devices have higher CM and DM currents than Si devices with higher operating frequency and switching speed; as a result, the flux density generated from Fig.9(a)–(c) is higher than Si devices [39]–[41].

Near magnetic coupling can be described using a mutual inductance model [42]. The induced voltage can be expressed as follows:

$$V_{\text{induced}} = M \cdot \frac{di}{dt} \quad (5)$$

where M is the mutual inductance between a noise circuit and a victim circuit and V_{induced} is the induced voltage in the victim circuit. The higher di/dt of WBG devices can cause higher induced voltage than Si devices.

C. Far-Field Radiated EMI

When the distance between the noise source and the victim is larger than $\lambda/2\pi$, it is considered as far-field region. Far-field coupling is also called the radiated EMI, which is
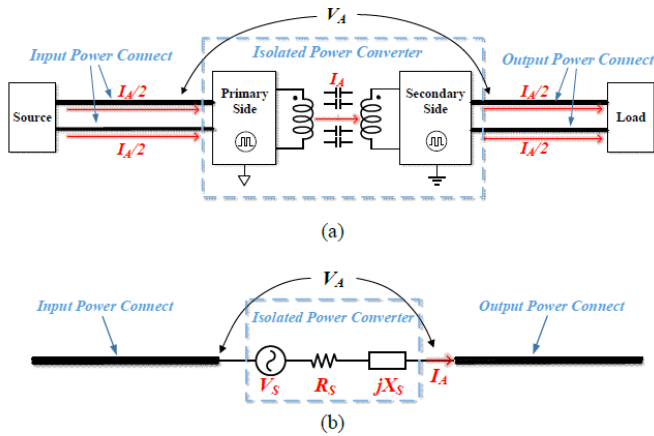
Fig. 9. Radiation mechanism of an isolated power converter. (a) CM current flowing through the parasitic capacitance between transformer windings. (b) Equivalent radiation model [50].

Fig. 10. Comparison of (a) spectra of switching voltage waveforms and (b) radiated electric field of converters with Si MOSFETs and GaN HEMTs [14].

measured with an antenna. The radiated EMI frequency range is from 30 MHz up to 1 GHz in FCC regulations and from 30 to 966 MHz in CISPR standards. In this article, the EMI noise from 30 MHz to 1 GHz is considered as radiated EMI.

The relationship between the far-field EMI and the near-field EMI of a power converter is discussed in [42]. A voltage-driven antenna model was proposed. The source of far-field radiation is the capacitive coupling between the cable and the printed circuit board (PCB) hot node. Zhang *et al.* [50], [51] developed an unintentional antenna model for isolated power converters and discussed the interactions between the antenna and the converter source impedance in Fig. 9. In Fig. 9, the power converter is modeled as a noise source and a source impedance. The input and output cables were modeled as a unintentional dipole antenna. The current flows through the unintentional antenna is the common-mode current of the converter. As analyzed in Section II, WBG devices have higher EMI spectrum than Si devices; as a result, the noise source spectrum of WBG devices is higher than that of Si devices. At the same time, the impedance of parasitic capacitance is inversely proportional to frequencies. With high switching frequencies, the noise of WBG devices will propagate through paths with reduced impedance. Consequently, the noise current flowing through the unintentional antenna is high and leads to high radiated EMI noise. As shown in Fig. 10, the radiated EMI noise of GaN HEMTs is 25 dB higher than that of Si MOSFETs from 200 to 300 MHz [14].

In [45], a time-domain measurement was conducted to analyze the radiated EMI. Ringing during switching transients was analyzed and compared with the measured far-field radiated EMI. It is proven in [47] and [48] that the ringing during switching transients increase radiated EMI at these oscillation frequencies.

IV. EMI REDUCTION TECHNIQUES FOR WBG DEVICES

Based on the previous review, WBG devices have higher conductive and radiated EMI than Si devices. While almost every EMI mitigation techniques developed for Si devices can be used in WBG devices, special attention must be paid for
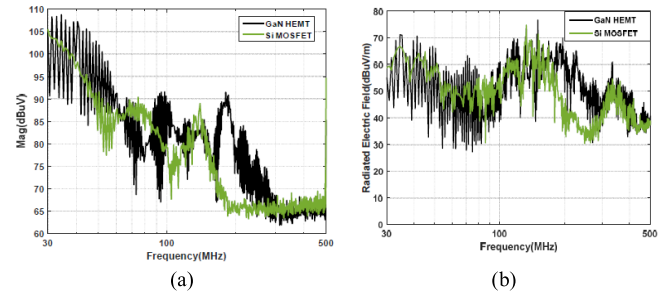
WBG devices. Solutions that were specifically designed for WBG devices are to be reviewed in this section. The mitigation approaches are classified as two major groups: 1) reducing EMI from the noise source side and 2) reducing EMI noise on the propagation path.

A. EMI Reduction From EMI Sources

As analyzed in Section II, the switching voltage waveform of WBG devices can be analyzed using asymmetrical trapezoidal waveforms superposed with oscillations during transient. The EMI mitigation techniques were also developed according to this.

The EMI of WBG devices can be reduced by slowing down the switching speed or optimize the switching process. As discussed in Section II, the switching speed is determined by junction capacitance and gate resistors. In [13], different ON- and OFF-gate resistors are used to change switching speed. Increasing the value of the gate resistor can reduce switching speed but with reduced efficiency. A tradeoff must be made.

Active gate drive (AGD) technique was proposed to reduce EMI while maintaining high efficiency. In [56], a novel AGD was proposed for SiC MOSFETs. Four gate resistors are used in different switching stages during a switching transient. Optimal gate resistance based on the oscillation equivalent circuit developed in [25] was calculated. Shahverdi *et al.* [59] also proposed an active gate driving technique with closed-loop control to improve the dynamics of SiC devices. A 6.7-GHz AGD was designed for GaN FETs in [57]. The AGD proposed in [57] has a very high resolution. It has the main driver with 2^8 resistance level and a fine driver with 2^6 resistance level. Because of this, the AGD can control the gate resistance very precisely. As shown in Fig. 11, by controlling the pull-up and pull-down strength of the driver, the two proposed active driving strategies can reduce switching speed at the desired time period as well as oscillations. Both conductive and radiated EMI noises can be controlled. As shown in Fig. 11, compared with the driving with constant gate resistance, the EMI noise with AGD can reduce EMI noise by 13 dB at 200 MHz and 10 dB at 1 GHz.

Other than AGDs, an aperiodic modulation technique was proposed in [60]. Modulation techniques were reviewed in [60]. Aperiodic modulation technique was explained and implemented in a GaN HEMT H-bridge-based impedance
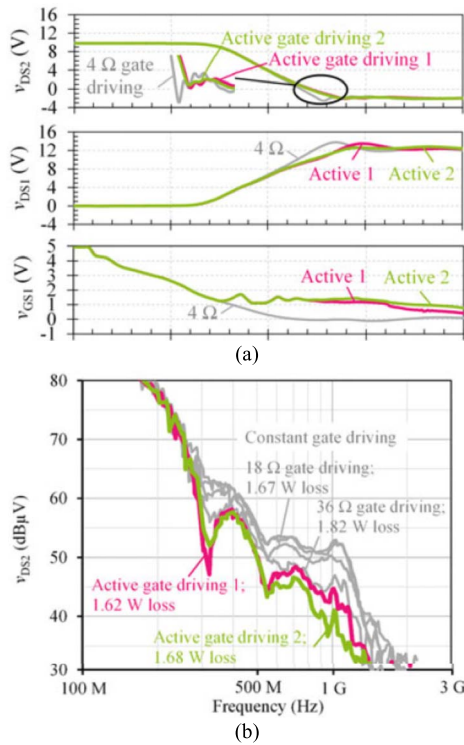
Fig. 11. (a) Switching waveforms of different switching strategies and (b) corresponding spectrum envelopes [56].
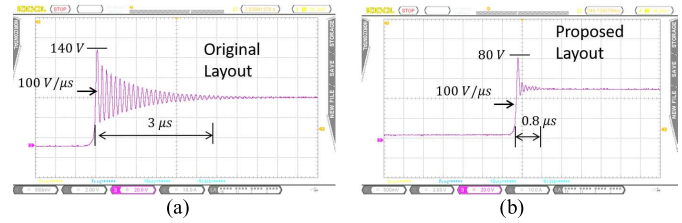

Fig. 12. Voltage waveforms during turn-off transient of the original and proposed layout under (a) turn-off voltage of the original layout under 50-V/30-A test and (d) turn-off voltage of the proposed layout under 50-V/-30 A test.

source converter. A modulation technique was proposed in [61] to eliminate the pulsewidth mismatch in the interleaved SiC PV inverter. With the proposed modulation technique in [61], an average reduction of 9 dB can be achieved.

Besides active techniques such as AGD and modulation techniques, passive techniques were also employed to reduce EMI. As presented in Sections II and III, WBG devices are sensitive to parasitic inductance [23]. To reduce the EMI caused by voltage and current ringing, the most direct and effective way is to minimize the parasitic inductance inside the current commutation loops. Over the years, reducing parasitic inductance has been an important topic in device and power module packaging. Different techniques proposed to reduce EMI for WBG devices and power modules are summarized in Table IV.

For the packaging of discrete devices, [62]–[66] proposed several packaging improvements for cascode GaN HEMT. A package parasitic inductance extraction technique was developed in [62]. In [63], a stacked die packaging with a compensating capacitor was proposed. The parasitic inductance between the Si MOSFET and GaN HEMT is reduced. Masuda et al. [67] and Ibuchi et al. [68] proposed the package layout for SiC MOSFETs. Using a near-field scanning technique, the wiring patterns are optimized.

In high-power applications, power modules are widely used. The WBG bare dies are usually connected via wire bonds inside the power module. The wire bond on direct bond copper (DBC) is a mature manufacturing process that has been used in the industry for years, and its total cost, thermal performance, and robustness have been proved to be good.

However, the large parasitic inductance of the wire bonds and the 2-D packaging structure cause high EMI for WBG devices.

As summarized in Table IV, many articles proposed the techniques to reduce parasitic inductance inside power modules. Some proposed techniques to improve layout inside the package to reduce parasitic inductance for wire bond on DBC power modules. Others proposed 2.5-D or 3-D packaging techniques. However, limited by the bonding technology, although the 3-D structure has the lowest inductance, it is difficult to fabricate and the cost is very high. As a result, they are difficult for mass production. Other packaging considerations and detailed comparison between different technologies and layouts are summarized in [83] and [84].

As shown in Table IV, the tradeoff between fabrication difficulty and parasitic inductance is obvious. Low parasitic inductance almost always comes at the cost of high fabrication difficulty. Particularly, in [28], a mutual inductance cancellation technique is proposed. The layout of a multichip SiC power module is designed so that the magnetic flux generated by each pair of paralleled branches can cancel each other. The total parasitic inductance can, therefore, be reduced without increasing fabrication difficulty. As shown in Fig. 12, the voltage overshoot and oscillation are effectively reduced.

In [23], [71], [72], and [81], decoupling capacitors were added inside the power module very close to power devices to reduce the area of current commutation loop. However, capacitors increase cost and the complexity of the module.

When improving packaging is not an option, various damping techniques were also proposed to reduce voltage and current oscillations. Traditional damping techniques, including RC snubbers and ferrite beads, are still effective for WBG devices. The use of RC snubbers was analyzed in [15], [24], [25], and [93]. The design of RC snubber is analytically discussed in [35]. The comparison of RC snubber and ferrite beads was made in [24].

While an RC snubber is easy to implement, ferrite beads presented the advantages of HF damping ability and higher efficiency [22], [20], [93] than RC snubbers. Both damping schemes must sacrifice a certain amount of efficiency to reduce EMI. The tradeoffs were discussed in [20], where different combinations of Si and SiC devices with different ferrite bead implementations were investigated. The effectiveness of ferrite beads is shown in Fig. 13. With ferrite beads, the spike at oscillation frequency (15 MHz) is effectively reduced by 15 dB. A novel damping scheme was proposed in [22].

TABLE IV

PARASITIC INDUCTANCE REDUCTION TECHNIQUES

| Reference	Bonding technology	Feature	Reduction techniques	Manufacturing difficulty	Parasitic inductance	Device power rating in the papers (Voltage /Current)
[71]	Solder on PCB	Low power GaN half bridge	Multiloop technique	Low	Medium	12 V/8.8 A
[67] [68]	Wire bond on DBC	Single-chip SiC half bridge	Optimized wiring pattern Decoupling capacitors	Low	Medium	650 V/ 10 A
[23]		Multichip SiC half bridge	Power loop area reduced by adding decoupling capacitors	Low	Medium	1200 V/ 120 A
[72]			Antiparallel connection of phase legs	Low	Medium	1200 V/ 360 A
[28]			Mutual inductance cancellation technique	Low	Low	1200 V / 300 A
[73] [74]	Wire bond on PCB		Trace length reduced by Via-enabled 3D structure	Medium	Low	1200 V/ 24 A 1200 V/ 120 A
[70]	Hybrid packaging	Single chip SiC module	Wire bond length reduced	Medium	Medium	1200 V/ 5 A
[53] [75] - [78]	planar packaging	SiC power modules	Wire bonds eliminated with planar structure	High	Low	1200 V/ 200 A
[54]		SiC Diode module				1200 V/ 20 A
[79]	Press-pack	SiC power modules	Wire bonds eliminated by press-pack technology	High	Low	1200 V / 200 A
[80]	SMD on PCB	GaN buck converter	Wire bonds eliminated by surface mount PCB	Low	Low	600 V /30 A
[81]	Conductive epoxy	SiC half bridge	Power loop area minimized in 3D structure	Highest	Minimum	1200 V /360 A
[82]	Vapor phase solder	GaN intelligent power module	Wire bonds eliminated by Via-enabled 3D structure	Medium	Low	650 V/ 30 A
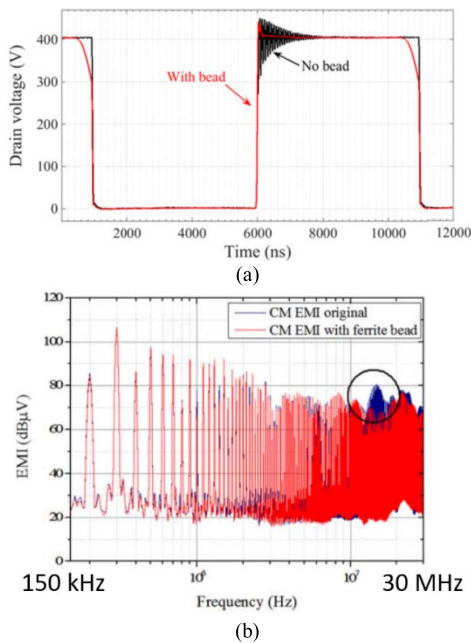
Fig. 13. (a) Switching waveforms and (b) measured CM noise of SiC converter with and without ferrite bead damping [15].

The concept of coupled Rogowski coil was used to increase impedance at high frequencies.

For bridge structure used in inverters and motor drives, a split output structure was proposed. EMI benefit was reported in [29] and [90], as oscillations were mitigated. However, the split output structure requires additional inductors, which increase cost and reduce efficiency. Velander *et al.* [91]

proposed a low-loss *dv/dt* filter concept. The parasitic inductance of cables was utilized and involved in the filter design. Although the concept is very inspiring, the applications of the *dv/dt* filter are limited since it targets to reduce the switching speed only.

As for radiated EMI, there were a few articles addressing how to reduce noise specifically for WBG devices. Hariya *et al.* [46] discussed the near-field coupling between a planar transformer and GaN HEMTs, but the discussion focused on the eddy current loss in the device channels.

B. EMI Reduction Along EMI Propagation Paths

Many techniques are developed to reduce EMI noise on EMI propagation paths. These techniques are summarized in Table V. For power electronics systems with WBG devices, the EMI propagation paths are very similar to the systems with Si devices. Techniques developed for Si devices [27], [94] can still be applied to WBG devices to reduce low-frequency noise. The general balance technique proposed in [94] is widely used to mitigate CM noise in power electronics system. CM noise generated in the GaN switched-capacitor converter was studied and reduced using the general balance technique in [95]. The principle of general balance technique is to manipulate the path impedance to form a balanced Wheatstone bridge, so the CM current can be canceled. From experimental results in the abovementioned works, a balanced structure can greatly reduce conductive CM noise. An up to 30-dB reduction from 150 kHz to 30 MHz is reported in [95] for a GaN switched-capacitor application. However, the effectiveness of balance technique depends on the accuracy of extracted impedances.

TABLE V
EMI REDUCTION TECHNIQUES ON EMI PROPAGATION PATHS

Reference	Type of EMI that can be reduced	Feature	Reduction methods
[35]	Conductive EMI	SiC JFET motor drive	Separate heat sinks
[85]		SiC inverter	Digital EMI filter
[94] [95]		GaN switched capacitor converter	Impedance balancing
[96]		GaN HEMT power module	CM and DM capacitors
[97]		SiC JFET inverter	Integrated CM capacitors
[98] – [99]		SiC power modules	CM and DM EMI filters
[103] - [105]		GaN HEMT converters	
[106]		SiC motor drives	
[39]	Near field emission	Multichip SiC power module	Inversed current loop direction
[41] – [44]		Passive components	Inductor design to reduce near magnetic field emission
[53]	Radiated EMI	SiC planar power module	Double sided DBC shielding
[50]		GaN HEMTs dual active bridge	CM capacitor
[49]		Buck converters	Ground inductor

The impedance may not be easily modeled or accurately balanced in radiated EMI range (>30 MHz), where HF noise may be significant for WBG devices.

Other than balancing, [35] investigated separating heatsinks in motor drive applications to reduce both CM and DM conductive EMIs. The separated heatsinks decoupled the interaction between upper and lower switches in a bridge, so it reduces the oscillations and DM EMI. It can also separate the interactions between bridge legs, so CM noise can be reduced. The effect of heatsink on EMI is also discussed in [3].

Besides various efforts to reduce EMI noise, EMI filters can be unavoidable in many applications. CM capacitors were integrated into a module [97], providing in-module EMI filtering. Different EMI filters and their effectiveness were discussed in [100]–[104]. Other than traditional EMI filters, a digital active EMI filter is proposed in [85]. Active filters can reduce the size of passive filters but has issues, including high cost, stability issues, limited attenuation performance [105], and gain bandwidth [106]. Digital active filters can save cost by utilizing the existing digital controller in high power electronics systems. With the help of improved digital processing techniques such as FPGA, the accuracy of the injected signal can be improved. However, limited by its sampling frequency, the benefits of digital active filter diminish at high frequencies.

Techniques to reduce near-field emission from magnetic components can be applied to the systems with either Si or WBG devices. Various structures are proposed in [41]–[44] for inductors and transformers to reduce the near magnetic field emission. These techniques can be applied to WBG device applications. For radiated EMI, it has been proven that CM current is the main cause of radiation [40]. As a result, the techniques to reduce CM current, including grounding inductor [49] and Y capacitor [50], have been proven effective.

V. EMI-RELATED RELIABILITY ISSUES INSIDE POWER CONVERTERS WITH WBG DEVICES

Other than the general EMI emission issues discussed in Sections II–IV, the fast switching speed of WBG power
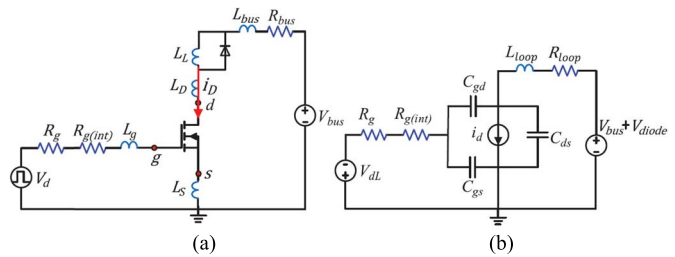

Fig. 14. (a) Equivalent circuit of a chopper circuit with SiC MOSFET under clamped inductive load. (b) Simplified circuit during turn-off process [23].

devices and their unique device structures also raise reliability concerns inside the power converters. Some EMI-related reliability issues and techniques to improve the reliability are summarized in this section. The reliability issues discussed in this section are focused on EMI-related issues. Other factors, such as the aging effect on power device and temperature impact, are not included.

A. Reliability Issues Caused by Voltage and Current Overshoot

As discussed in Section II, the switching voltage ringing in power converters with WBG devices is more severe than that with Si devices [22]–[24]. For a copper circuit in Fig. 14, the overshoot spike of the drain-to-source voltage during turn-off transient is given by (6), where L_{loop} is the total parasitic inductance of the power loop, I_D is the load current, and g_{fs} is the transconductance of the device. V_{th} and V_{dL} are the threshold voltage and driver low-level voltage, respectively. C_{gd} is the gate-to-drain capacitance, R_g and $R_{g(\text{int})}$ are the external and internal gate resistor, respectively

$$V_{\text{max}} = \sqrt{\frac{2L_{\text{loop}}I_D\left(\frac{I_D}{g_{\text{fs}}} + V_{\text{th}} - V_{\text{dL}}\right)}{C_{\text{gd}}(R_g + R_{g(\text{int})})}}. \tag{6}$$

As discussed in Section II, WBG devices have smaller C_{gd} than Si devices. According to (6), with the same power loop inductance, the same operating voltage, the same load current, and the same driving condition, the peak turn-off overshoot

voltage V_{max} of WBG devices is higher than that of Si devices. WBG devices must endure repetitive higher voltage stress than Si devices. When the overshoot voltage is above the breakdown voltage, the devices could be damaged.

Other than voltage overshoot, there will be an overshoot current flowing through the power device during device turn-on transient [30]. This is caused by the reverse recovery of the diode as well as the parasitic inductance and capacitance in the power loop. As discussed in Section II-A, the reverse recovery current is determined by the diode reverse recovery characteristics. In cases where the SiC Schottky diode is used, the reverse recovery current is nearly eliminated. However, because of the high dv/dt across the diode, the current flowing through the junction capacitance is large. At the same time, the load current flowing through the parasitic inductance determines the initial condition of the oscillation in the power loop. In high-power applications where both dv/dt and load current are high, the overshoot current caused by these two factors outweighs the current overshoot caused by the diode reverse recovery. In the case in [30], when the load current is higher than 250 A, the overshoot current of SiC MOSFETs becomes higher than that of Si IGBTs. The overshoot current causes additional power loss on the devices, raising reliability concerns.

B. Sustained Oscillation Caused by False Triggering

The voltage and current overshoot and ringing discussed previously are caused by high switching speed associated with parasitic parameters in the power loop. At the same time, the drive loop and power loop are coupled via gate-to-drain capacitance (Miller capacitance) and common source inductance [108]. Consequently, the voltage and current ringing in the power loop will interfere with the gate voltage. This interference could lead to sustained oscillation in the power converter, which causes a system failure. The sustained oscillation is more likely to happen to the system with WBG devices [66], [107]–[109].

There are two necessary conditions for sustained oscillations. The first is the additional energy source, for example, the false triggering of the power device. After falsely turned on, the power device keeps drawing energy from the power source, creating a condition where the oscillation seems to be "perpetual." The second is the underdamped environment created by the parasitic parameters. In this way, the oscillation could become divergent under any excitation. These two conditions will be discussed individually.

Compared to Si devices, GaN FETs are more prone to suffer from false triggering because of the low threshold voltage. In a converter with a single GaN FET, the device could be falsely turned on by the switching operation of itself.

In a boost converter in Fig. 15, during turn-off transient, because the drain-to-source voltage of the GaN FET rises quickly, the induced current flows through the Miller capacitance. At the same time, the quick decrease in drain current induces a voltage on the common source inductance L_s. The induced voltage and the current flowing through Miller capacitance lead to the increased gate-to-source voltage. When
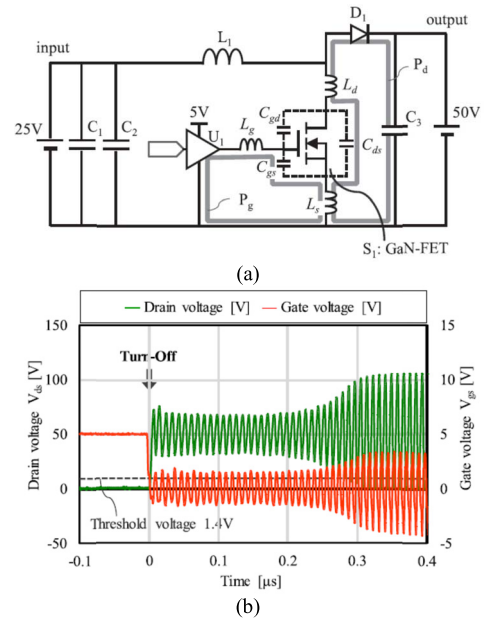

Fig. 15. (a) Boost converter with GaN FET and (b) sustained oscillation in power loop and drive loop [108].
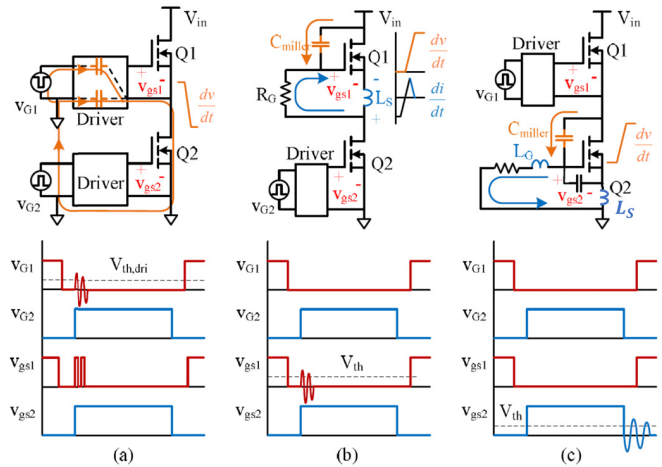
Fig. 16. Equivalent circuit and typical waveforms of the common instability problems [17]. (a) PWM signal noise. (b) Crosstalk effect. (c) Gate voltage oscillation.

the gate-to-source voltage rises above the threshold voltage, which is more likely for GaN FETs due to their low threshold voltage, the device is falsely turned on. The system will risk sustained oscillation.

For a bridge structure that is composed of top switch (TS) and bottom switch (BS), the false triggering not only occurs to the switch being actively driven but also to the complimentary switch that should be kept OFF. The false triggering in a half-bridge structure can be caused by many factors. The three most common factors are illustrated in the half bridge with enhancement-mode GaN HEMTs in Fig. 16 [17].

In Fig. 16, the high dv/dt and high di/dt during the switching transients lead to false triggering. First, the initial current flows from TS's source to drain when the BS is turned on and the TS V_G is 0 V. During the transient, the drain-to-source

voltage of the TS rises quickly. High dv/dt can distort the PWM signal through parasitic capacitance between the power circuit and the driver, as shown in Fig. 16(a). The PWM signal disturbance could trigger a false driving signal and turn on the TS by mistake. Second, during the same transient, displacement current will flow through the Miller capacitance of the TS and increase the gate voltage of the TS, as shown in Fig. 16(b). At the same time, the voltage induced on common source inductance L_s will also cause a disturbance in the gate loop of the TS. Finally, during the turn-off transient of the BS, the gate voltage of the BS can be raised by the current flowing through its Miller capacitance and the voltage induced on common source inductance, as shown in Fig. 16(c). The gate voltage interference of the BS is similar to that in the boost converter in Fig. 15. It can be concluded that all three factors of the false triggering are caused by fast switching speed. Consequently, WBG devices are more likely to be falsely turned on in half-bridge circuits.

Other than fast switching speed, the structures of some WBG devices could also risk sustained oscillations. The enhancement-mode GaN HEMTs have a unique symmetrical structure. When in reverse conduction, the device operates in the saturation region. As a result, different from diodes or the body diodes of MOSFETs, the current flows through the channel is governed by the gate-to-drain voltage. In a bridge structure, when both devices are enhancement-mode GaN HEMTs, the scenario where one device is turned off and the other device is reversely conducting current is very common. Instead of being falsely turned on, enhancement-mode GaN HEMTs are reversely turned on in normal operation. However, when the GaN HEMT is reversely turned on, the channel current is a controlled current source. The device could also draw energy from the source, providing the same condition as a falsely turned on device. In a bridge circuit with enhancement-mode GaN HEMTs, the system would risk sustained oscillation when one device is turned off and the other is reversely turned on. Other than enhancement GaN HEMT, the occurrence of sustained oscillation is also related to the structure of cascode GaN HEMTs. As discussed in Section II, cascode GaN HEMT has a low-power Si MOSFET between the gate and the source of the depletion-mode GaN HEMT, making it a normally off device. It has been studied in [66] that during the turn-off transient, the current oscillation in the power loop could increase the drain-to-source voltage of the Si MOSFET and hence falsely turns on the depletion-mode GaN HEMT. Once the GaN HEMT is turned on, it starts to draw energy from the dc voltage source. The reason for this sustained oscillation in the cascode GaN HEMTs was concluded as a junction capacitance mismatch between Si MOSFET and GaN HEMT in [66].

As mentioned earlier, the other necessary condition for sustained oscillation is the parasitic parameters. After the false triggering occurred, the channel current becomes a controlled current source and it injects energy into the oscillation tank. Certain stability criteria must be satisfied to sustain the oscillation. In [108]–[110], equivalent small-signal circuits are derived for the oscillation. The oscillator model of the clamped inductive load test circuit in Fig. 17(a) is derived in
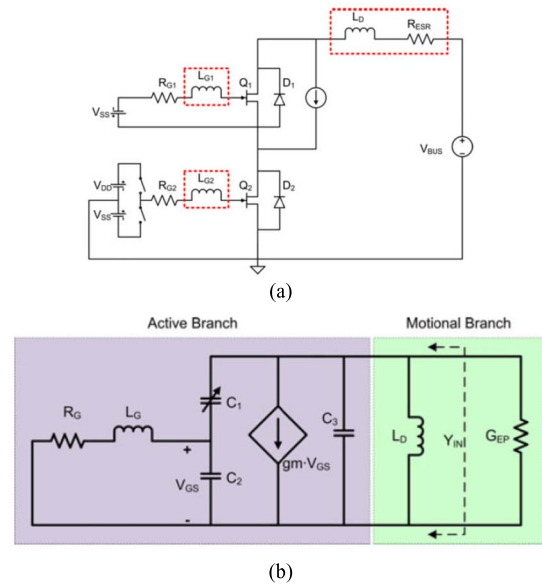

(a)

(b)

Fig. 17. (a) Clamped inductive load test circuit (BS is being actively driven and TS is kept OFF). (b) Equivalent small-signal model [109].

Fig. 17(b) [109], where the parasitic inductance of power loop is L_d, and G_{EP} is the effective power loop conductance. In this case, the sustained oscillation condition is that the real part of Y_{IN} is smaller than $-G_{EP}$.

In general, to determine whether the sustained oscillation occurs, three steps should be followed. First, identify the device that was falsely triggered or reversely turned on in the circuits. Second, develop the small-signal model for the oscillation. Third, calculate the loop gain. If the real part of the loop gain is larger than the unit at the frequency where the imaginary part is zero (Barkhausen criterion) or the closed-loop transfer function has right plane poles (Nyquist criterion), the sustained oscillation will happen.

C. Gate Reliability

Another concern of device failure is the gate voltage. If the gate voltage of the device is out of the safe operating region, the device is under the risk of failure. Several characteristics make the WBG devices more susceptible to gate voltage failure

In Fig. 18(a), due to the unique structure of cascode GaN, the connections between Si MOSFET and GaN HEMT inevitably introduce parasitic inductance. During device switching transients, the parasitic inductance L_{int1}, L_{int2}, and L_{int3} resonate with the junction capacitance C_{ds} of Si MOSFET and C_{gd} of GaN HEMT. The oscillating voltage could be out of the safe operating region of the GaN HEMT [119]. In Fig. 18(b), the gate voltage of GaN HEMT oscillates below the breakdown voltage, -35 V. The device is under risk.

For SiC MOSFET, the safe operating region of gate voltage is from -5 to 20 V, which is smaller than Si IGBTs (from -20 to 20 V). During high-speed switching transient, positive and negative voltages will be induced due to the Miller capacitance and common source inductance [30]. The gate voltage
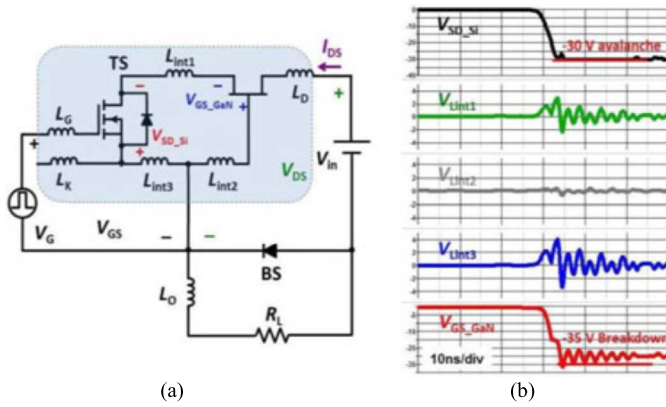
Fig. 18. (a) Equivalent circuit of a boost converter with cascode GaN HEMT as TS and diode as BS and (b) simulated waveforms under 400-V/12-A turn-off transient [63].
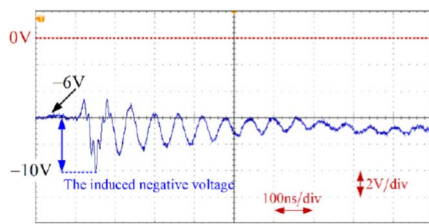

Fig. 19. Measured typical-induced negative gate voltage [30].

disturbance would be more likely to exceed the maximum negative limit for SiC MOSFET, as shown in Fig. 19. When the gate voltage is out of the safe operating region, the lifetime of SiC MOSFET could be compromised [111].

D. Techniques to Address the Reliability Issues

The existing and possible techniques to increase the EMC reliability of power converter with WBG devices will be discussed here. While reducing the switching speed by increasing the gate resistor could increase the EMC reliability of the converter, it also sacrifices efficiency. Because of this, techniques that can increase the EMC reliability without increasing the gate resistors are reviewed and presented in this section.

To deal with the voltage and current overshoots, the most direct way is to optimize the parasitic parameters. By reducing the parasitic inductance inside the power loop, both voltage and current oscillations will be reduced. Specifically, since the initial energy stored in parasitic inductance leads to current overshoot in power modules with WBG devices, reducing parasitic inductance will be the most effective way to reduce voltage and current overshoots. Various techniques to reduce parasitic inductance are listed in Table IV.

To address the sustained oscillation issue, the first way is to prevent false triggering. Normally, in industrial practice, false triggering should be avoided by all means. From the discussion in Section V-B, the critical parameters that cause false triggering are the parasitic capacitance between power loop and driver, common source inductance, and Miller capacitance. Techniques have been developed to reduce the influence of these parameters.

For the PWM signal distortion caused by the parasitic capacitance between the power circuit and driver, three techniques are proposed and tested in [120]. An additional shielding layer placed below the driver was proven to be the most effective.

For the coupling due to the common source inductance, using the Kelvin source connection is an effective way to decouple the drive loop and power loop [6]. With the Kelvin connection, the drive loop is almost independent of the power loop. As a result, the interference caused by common source inductance is reduced. It should be pointed out that applying the Kelvin connection to multichip power modules increases the complexity of the package layout. The power loop and drive loop layouts of each paralleled chip need to be carefully designed to avoid current unbalance [7]. In [66], an additional capacitor is integrated inside the package of cascode GaN HEMT so that there is no capacitance mismatch between the depletion-mode GaN HEMT and Si MOSFET. The divergent oscillation can be avoided.

Because the Miller capacitance is an intrinsic device characteristic, there are no techniques to reduce the Miller capacitance once the device is fabricated. Therefore, the interference caused by the Miller capacitance is addressed with driver design. In [113], two assistive circuits were proposed to suppress the crosstalk effect due to the Miller capacitance: active Miller clamp circuit and gate voltage control circuit. The two time-sequence-controlled circuits could suppress the induced gate voltage, hence preventing false triggering. In [114], four additional capacitors were added to address the crosstalk effect. The capacitors are aimed to provide low impedance paths for the charging current. It should be noted that with the capacitors in [114], the turn-off gate resistor is bypassed, so the turn-off speed cannot be controlled anymore. Other driver-assistive circuits are proposed in [106]–[108]. These driver-assistive circuits can effectively prevent false triggering but will increase the driver's complexity and cost.

As discussed in Section V-B, false triggering does not necessarily lead to sustained oscillation. The stability of the system also depends on the stability criterion. The stability criterion is determined by parasitic parameters. Therefore, to prevent sustained oscillation, the small-signal model can be developed according to [107]–[110]. Parasitic parameters should be controlled so that the stability criterion is met. Deriving small-signal models for different circuit topologies and calculating stability criterion could be time-consuming. As a result, several rules are summarized in this article to save time.

1) For the power module with a bridge structure, the drive loop parasitic inductance should be kept as small as possible.
2) For single active switch power converters, the oscillation frequency of power loop ($f_{\text{power}} = 1/((L_{\text{loop}}C_{\text{oss}})^{1/2})$ and drive loop ($f_{\text{drive}} = 1/((L_g C_{\text{iss}})^{1/2})$) should be away from each other to improve stability. If it is difficult, one of the two following conditions should be met: $(L_d/C_{\text{gs}}) < (L_s/C_{\text{gd}}) < (L_g/C_{\text{ds}})$ or $(L_g/C_{ds}) < (L_s/C_{\text{gd}}) < (L_d/C_{\text{gs}})$.
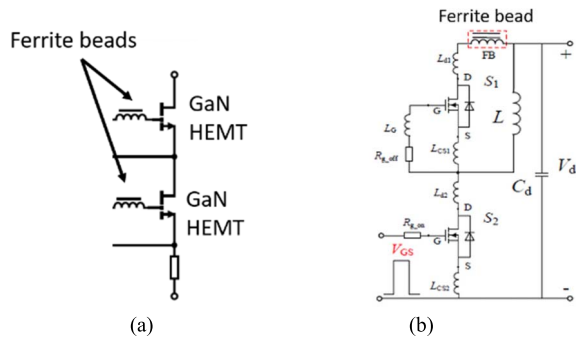
Fig. 20. Examples of applying ferrite beads to a bridge circuit. (a) Ferrite beads in the drive loop [82]. (b) Ferrite beads in the power loop [93].

3) Ferrite beads with HF power loss can be added to the drive loop and power loop to damp the oscillations, as shown in Fig. 20.
4) Antiparallel diode can be added to the enhancement GaN HEMT in the power module with a bridge structure to prevent the devices to reversely turn on.

To increase gate EMC reliability, it is important to keep the gate voltage within the safe operating region. In [10], a stacked die package structure is proposed to mitigate the gate voltage oscillation. In [117], a driver circuit is proposed to suppress the negative voltage spikes. A p-n-p transistor is added to provide a low impedance path for the displacement current. Using a small diode between the gate and the source of a SiC MOSFET die helps clamp the negative gate voltage.

It can be concluded that the reliability of power converters with WBG devices is highly sensitive to the parasitic parameters. Because of the high switching speed, large parasitic inductance is detrimental to all the EMI-related reliability issues. As a result, special attention must be paid to reduce the power loop and drive loop inductance and reduce the coupling between the drive loop and the power loop. Special techniques need to be developed for WBG devices regarding layout and package design that were not necessary for classical power devices because they already have satisfactory performance.

VI. CONCLUSION

In this article, a detailed survey of the characteristics of WBG power devices and the related EMI issues was conducted. EMI reduction techniques for the systems with WBG devices are reviewed and summarized. Additionally, EMI-related reliability issues inside power converters with WBG devices have been reviewed. Techniques to increase the reliability of power converters with WBG devices are summarized. To successfully design a power electronics system with WBG devices for good EMC performance, several steps should be followed.

1) When designing with discrete WBG switches, the devices with the Kelvin connection should be selected if possible. When designing the converter with bare dies, the drive loop and power loop should be separated. The common source inductance should be kept as small as possible. Rules in Section V-D should also be followed to increase the reliability of the system.

TABLE VI
EMI ISSUES AND POSSIBLE FUTURE RESEARCH TOPICS

EMI Issues	Future Research Topics
Conductive EMI (150 kHz – 30 MHz)	Aim: To reduce EMI noise source without sacrificing efficiency Topics: Advanced driving strategy, switching frequency modulation
	Aim: To reduce parasitic oscillations Topics: Package optimization, damping scheme
Radiated EMI (far field) (>30MHz)	Aim: To understand the generation and propagation of radiated EMI Topics: Modeling and measurement of radiated EMI
	Aim: Reduce radiated EMI Research: switching frequency modulation, advanced driving scheme, filter components with large high frequency impedance, shielding techniques, grounding techniques, PCB layout, packaging optimization,
Near field coupling	Aim: Influence of near field coupling to conductive and radiated EMI Topics: Modeling near field couplings
	Aim: Influence of near field coupling on the reliability of power converters Topics: Near field coupling between the power loop and the drive loop
	Aim: To reduce the near field couplings Topics: Passive components with low near field emission and near field immunity, shielding techniques, cancellation technique

2) During the converter layout design process, the parasitic inductance of the power loop and drive loop should be designed as small as possible. Depending on the power rating and acceptable fabrication difficulty (cost), techniques can be selected from Table IV.
3) The conductive EMI spectrum should be measured. If spikes appear at HF range (such as the spectrum in Fig. 13), it means that the voltage and current oscillation may still be large. If confirmed, the damping techniques summarized in Section IV can be applied to the power loop. At the same time, slowing down the switching speed or controlling the switching speed with AGD is also effective. Applying damping techniques and slowing down the switching speed is usually a tradeoff process; the increased power loss needs to be weighted.
4) The conductive EMI spectrum should be measured based on the required standards. If EMI noise near switching frequency is above standard, EMI filters should be added. Depending on how much attenuation is needed, techniques can be selected from Table V. If EMI noise at high frequencies is above the standard but not caused by the oscillation in step 3, it is usually caused by the fast switching speed. Techniques, such as increase gate resistor and an AGD, can be applied.
5) If required, the radiated EMI noise should be measured. If the radiated EMI is higher than the EMI standards, additional reduction techniques should be applied. As mentioned, techniques to address the radiated EMI noise from power converters with WBG devices are still being developed.

The superior properties of WBG materials have the potential to increase switching speed, reduce power loss, and operate at higher switching frequencies than Si devices. At the same time, these characteristics may cause higher EMI noise and more serious reliability issues than Si devices. This has brought new challenges as well as new research opportunities. The challenges brought by WBG devices and possible future research topics are summarized in Table VI. Different from conductive EMI research, there are still very few studies conducted to investigate radiated EMI and near-field coupling for the systems with WBG devices. At the same time, the issues of near-field and radiated EMI due to WBG devices are more severe than those due to Si devices. Consequently, the systems using WBG devices are prone to over EMI standards. The relationship between near-field coupling and far-field radiation has not been thoroughly modeled currently for power electronics systems. Meanwhile, because the power converters with WBG devices operate at high frequencies and have high speed, the coupling mechanism between the drive loop and the power loop may no longer be limited to the Miller capacitance and common source inductance. The interference in the drive loop could be induced due to the near magnetic field or near electric field couplings. The research on the near-field coupling is important because it can influence the reliability of power converters. Therefore, future studies on the modeling and reduction of near-field couplings and radiated EMI are urgently needed for taking advantage of WBG devices.

REFERENCES

[1] J. Millan, P. Godignon, X. Perpina, A. Perez-Tomas, and J. Rebollo, "A survey of wide bandgap power semiconductor devices," *IEEE Trans. Power Electron.*, vol. 29, no. 5, pp. 2155–2163, May 2014.

[2] E. A. Jones, F. F. Wang, and D. Costinett, "Review of commercial GaN power devices and GaN-based converter design challenges," *IEEE J. Emerg. Sel. Topics Power Electron.*, vol. 4, no. 3, pp. 707–719, Sep. 2016.

[3] A. N. Lemmon, R. Cuzner, J. Gafford, R. Hosseini, A. D. Brovont, and M. S. Mazzola, "Methodology for characterization of common-mode conducted electromagnetic emissions in wide-bandgap converters for ungrounded shipboard applications," *IEEE J. Emerg. Sel. Topics Power Electron.*, vol. 6, no. 1, pp. 300–314, Mar. 2018.

[4] X. Huang, Z. Liu, Q. Li, and F. C. Lee, "Evaluation and application of 600 V GaN HEMT in cascode structure," *IEEE Trans. Power Electron.*, vol. 29, no. 5, pp. 2453–2461, May 2014.

[5] F. F. Wang and Z. Zhang, "Overview of silicon carbide technology: Device, converter, system, and application," *CPSS Trans. Power Electron. Appl.*, vol. 1, no. 1, pp. 13–32, Dec. 2016.

[6] Z. Chen, "Electrical integration of SiC power devices for high-power-density applications," Ph.D. dissertation, Virginia Polytech. Inst. State Univ., Blacksburg, VA, USA, 2013.

[7] A. K. Morya *et al.*, "Wide bandgap devices in AC electric drives: Opportunities and challenges," *IEEE Trans. Transport. Electrific.*, vol. 5, no. 1, pp. 3–20, Mar. 2019.

[8] B. J. Baliga, *Fundamentals of Power Semiconductor Devices*. New York, NY, USA: Springer, 2008.

[9] X. She, A. Q. Huang, Ó. Lucía, and B. Ozpineci, "Review of silicon carbide power devices and their applications," *IEEE Trans. Ind. Electron.*, vol. 64, no. 10, pp. 8193–8205, Oct. 2017.

[10] X. Yuan, S. Walder, and N. Oswald, "EMI generation characteristics of SiC and Si diodes: Influence of reverse-recovery characteristics," *IEEE Trans. Power Electron.*, vol. 30, no. 3, pp. 1131–1136, Mar. 2015.

[11] J. Wang, H. S. H. Chung, and R. T. H. Li, "Characterization and experimental assessment of the effects of parasitic elements on the MOSFET switching performance," *IEEE Trans. Power Electron.*, vol. 28, no. 1, pp. 573–590, Jan. 2013.

[12] H. Li *et al.*, "Influences of device and circuit mismatches on paralleling silicon carbide MOSFETs," *IEEE Trans. Power Electron.*, vol. 31, no. 1, pp. 621–634, Jan. 2016.

[13] D. Han, C. T. Morris, W. Lee, and B. Sarlioglu, "A case study on common mode electromagnetic interference characteristics of GaN HEMT and Si MOSFET power converters for EV/HEVs," *IEEE Trans. Transport. Electrific.*, vol. 3, no. 1, pp. 168–179, Mar. 2017.

[14] Y. Zhang, S. Wang, and Y. Chu, "Comparison of radiated electromagnetic interference (EMI) generated by power converters with silicon MOSFETs and GaN HEMTs," in *Proc. IEEE Appl. Power Electron. Conf. Expo. (APEC)*, Anaheim, CA, USA, Mar. 2019, pp. 1375–1382.

[15] T. Kim, D. Feng, M. Jang, and V. G. Agelidis, "Common mode noise analysis for cascaded boost converter with silicon carbide devices," *IEEE Trans. Power Electron.*, vol. 32, no. 3, pp. 1917–1926, Mar. 2017.

[16] X. Wang, Z. Zhao, Y. Zhu, K. Chen, and L. Yuan, "A comprehensive study on the gate-loop stability of the SiC MOSFET," in *Proc. IEEE Energy Convers. Congr. Expo. (ECCE)*, Cincinnati, OH, USA, Oct. 2017, pp. 3012–3018.

[17] K. Wang, X. Yang, L. Wang, and P. Jain, "Instability analysis and oscillation suppression of enhancement-mode GaN devices in half-bridge circuits," *IEEE Trans. Power Electron.*, vol. 33, no. 2, pp. 1585–1596, Feb. 2018.

[18] D. Han, S. Li, Y. Wu, W. Choi, and B. Sarlioglu, "Comparative analysis on conducted CM EMI emission of motor drives: WBG versus Si devices," *IEEE Trans. Ind. Electron.*, vol. 64, no. 10, pp. 8353–8363, Oct. 2017.

[19] D. Han and B. Sarlioglu, "Comprehensive study of the performance of SiC MOSFET-based automotive DC-DC converter under the influence of parasitic inductance," *IEEE Trans. Ind. Appl.*, vol. 52, no. 6, pp. 5100–5111, Nov./Dec. 2016.

[20] N. Oswald, P. Anthony, N. McNeill, and B. H. Stark, "An experimental investigation of the tradeoff between switching losses and EMI generation with hard-switched all-Si, Si-SiC, and all-SiC device combinations," *IEEE Trans. Power Electron.*, vol. 29, no. 5, pp. 2393–2407, May 2014.

[21] P. G. Neudeck, R. S. Okojie, and L.-Y. Chen, "High-temperature electronics—A role for wide bandgap semiconductors?" *Proc. IEEE*, vol. 90, no. 6, pp. 1065–1076, Jun. 2002.

[22] J. Kim, D. Shin, and S.-K. Sul, "A damping scheme for switching ringing of full SiC MOSFET by air core PCB circuit," *IEEE Trans. Power Electron.*, vol. 33, no. 6, pp. 4605–4615, Jun. 2018.

[23] Y. Ren *et al.*, "Voltage suppression in wire-bond-based multichip phase-leg SiC MOSFET module using adjacent decoupling concept," *IEEE Trans. Ind. Electron.*, vol. 64, no. 10, pp. 8235–8246, Oct. 2017.

[24] I. Josifović, J. Popović-Gerber, and J. A. Ferreira, "Improving SiC JFET switching behavior under influence of circuit parasitics," *IEEE Trans. Power Electron.*, vol. 27, no. 8, pp. 3843–3854, Aug. 2012.

[25] T. Liu, R. Ning, T. T. Y. Wong, and Z. J. Shen, "Modeling and analysis of SiC MOSFET switching oscillations," *IEEE J. Emerg. Sel. Topics Power Electron.*, vol. 4, no. 3, pp. 747–756, Sep. 2016.

[26] S. Wang, F. C. Lee, and W. G. Odendaal, "Characterization and parasitic extraction of EMI filters using scattering parameters," *IEEE Trans. Power Electron.*, vol. 20, no. 2, pp. 502–510, Mar. 2005.

[27] S. Wang, "EMI modeling and reduction in modern power electronics systems," in *Proc. IEEE Symp. Electromagn. Compat., Signal Integrity Power Integrity (EMC, SI PI)*, Long Beach, CA, USA, Jul./Aug. 2018, pp. 1–44.

[28] B. Zhang and S. Wang, "Parasitic inductance modeling and reduction for a wire bonded half bridge SiC MOSFET multichip power module," in *Proc. IEEE Appl. Power Electron. Conf. Expo. (APEC)*, Anaheim, CA, USA, Mar. 2019, pp. 656–663.

[29] Q. Yan, X. Yuan, Y. Geng, A. Charalambous, and X. Wu, "Performance evaluation of split output converters with SiC MOSFETs and SiC Schottky diodes," *IEEE Trans. Power Electron.*, vol. 32, no. 1, pp. 406–422, Jan. 2017.

[30] L. Zhang, X. Yuan, X. Wu, C. Shi, J. Zhang, and Y. Zhang, "Performance evaluation of high-power SiC MOSFET modules in comparison to Si IGBT modules," *IEEE Trans. Power Electron.*, vol. 34, no. 2, pp. 1181–1196, Feb. 2019.

[31] A. Trentin, L. D. Lillo, L. Empringham, P. Wheeler, and J. Clare, "Experimental comparison of a direct matrix converter using Si IGBT and SiC MOSFETs," *IEEE J. Emerg. Sel. Topics Power Electron.*, vol. 3, no. 2, pp. 542–554, Jun. 2015.

[32] B. Sun, R. Burgos, and D. Boroyevich, "Common-mode EMI unterminated behavioral model of wide-bandgap-based power converters operating at high switching frequency," *IEEE J. Emerg. Sel. Topics Power Electron.*, vol. 7, no. 4, pp. 2561–2570, Dec. 2019.

[33] Y. Xie, C. Chen, Z. Huang, T. Liu, Y. Kang, and F. Luo, "High frequency conducted EMI Investigation on packaging and modulation for a SiC-based high frequency converter," *IEEE J. Emerg. Sel. Topics Power Electron.*, vol. 7, no. 3, pp. 1789–1804, Sep. 2019.

[34] L. Middelstaedt, B. Strauss, A. Chupryn, and A. Lindemann, "Investigation of the root causes of electromagnetic noise of an interleaved DC-DC converter with GaN or Si transistors and corresponding optimization strategies," *IEEE J. Emerg. Sel. Topics Power Electron.*, to be published.

[35] X. Gong and J. A. Ferreira, "Investigation of conducted EMI in SiC JFET inverters using separated heat sinks," *IEEE Trans. Ind. Electron.*, vol. 61, no. 1, pp. 115–125, Jan. 2014.

[36] X. Gong, I. Josifović, and J. A. Ferreira, "Modeling and reduction of conducted EMI of inverters with SiC JFETs on insulated metal substrate," *IEEE Trans. Power Electron.*, vol. 28, no. 7, pp. 3138–3146, Jul. 2013.

[37] P. Saini and M. Arora, "Microwave absorption and EMI shielding behavior of nanocomposites based on intrinsically conducting polymers, graphene and carbon nanotubes," *New Polym. Special Appl.*, vol. 3, pp. 73–112, Sep. 2012.

[38] G. Ala, M. C. D. Piazza, G. Tine, F. Viola, and G. Vitale, "Evaluation of radiated EMI in 42-V vehicle electrical systems by FDTD simulation," *IEEE Trans. Veh. Technol.*, vol. 56, no. 4, pp. 1477–1484, Jul. 2007.

[39] M. Wang, F. Luo, and L. Xu, "A double-end sourced wire-bonded multichip SiC MOSFET power module with improved dynamic current sharing," *IEEE J. Emerg. Sel. Topics Power Electron.*, vol. 5, no. 4, pp. 1828–1836, Dec. 2017.

[40] H. Chen, T. Wang, L. Feng, and G. Chen, "Determining far-field EMI from near-field coupling of a power converter," *IEEE Trans. Power Electron.*, vol. 29, no. 10, pp. 5257–5264, Oct. 2014.

[41] B. Zhang and S. Wang, "Analysis and reduction of the near magnetic field radiation from magnetic inductors," in *Proc. IEEE Appl. Power Electron. Conf. Expo. (APEC)*, Tampa, FL, USA, Mar. 2017, pp. 2494–2501.

[42] Q. Chen, Y. Pei, X. Yang, and Z. Wang, "Analysis and suppression of inductive interference in an active integrated power electronics module," *IEEE Trans. Compon. Packag. Technol.*, vol. 32, no. 4, pp. 724–733, Dec. 2009.

[43] Y. Chu, S. Wang, N. Zhang, and D. Fu, "A common mode inductor with external magnetic field immunity, low-magnetic field emission, and high-differential mode inductance," *IEEE Trans. Power Electron.*, vol. 30, no. 12, pp. 6684–6694, Dec. 2015.

[44] H. Zhang, B. Zhang, and S. Wang, "Integrated common mode and differential mode inductors with low near magnetic field emission," in *Proc. IEEE Energy Convers. Congr. Expo. (ECCE)*, Cincinnati, OH, USA, Oct. 2017, pp. 5375–5382.

[45] L. Middelstaedt and A. Lindemann, "Methodology for analysing radiated EMI characteristics using transient time domain measurements," *IET Power Electron.*, vol. 9, no. 10, pp. 2013–2018, Aug. 2016.

[46] A. Hariya *et al.*, "Circuit design techniques for reducing the effects of magnetic flux on GaN-HEMTs in 5-MHz 100-W high power-density LLC resonant DC–DC converters," *IEEE Trans. Power Electron.*, vol. 32, no. 8, pp. 5953–5963, Aug. 2017.

[47] O. Aouine, C. Labarre, and F. Costa, "Measurement and modeling of the magnetic near field radiated by a buck chopper," *IEEE Trans. Electromagn. Compat.*, vol. 50, no. 2, pp. 445–449, May 2008.

[48] L. Beghou, F. Costa, and L. Pichon, "Detection of electromagnetic radiations sources at the switching time scale using an inverse problem-based resolution method—Application to power electronic circuits," *IEEE Trans. Electromagn. Compat.*, vol. 57, no. 1, pp. 52–60, Feb. 2015.

[49] M. Laour, R. Tahmi, and C. Vollaire, "Modeling and analysis of conducted and radiated emissions due to common mode current of a buck converter," *IEEE Trans. Electromagn. Compat.*, vol. 59, no. 4, pp. 1260–1267, Aug. 2017.

[50] Y. Zhang, S. Wang, and Y. Chu, "Predicting far-field radiation with the emission models of power converters," in *Proc. IEEE Int. Symp. Electromagn. Compat. Signal/Power Integrity (EMCSI)*, Washington, DC, USA, Aug. 2017, pp. 797–802.

[51] Y. Zhang, S. Wang, and Y. Chu, "Investigation of radiated electromagnetic interference for an isolated high-frequency DC–DC power converter with power cables," *IEEE Trans. Power Electron.*, vol. 34, no. 10, pp. 9632–9643, Oct. 2019.

[52] H. Zhang, S. Wang, and Q. Wang, "Winding and air gap configurations for power inductors to reduce near magnetic field emission," in *Proc. IEEE Energy Convers. Congr. Expo. (ECCE)*, Cincinnati, OH, USA, Oct. 2017, pp. 903–910.

[53] A. Dutta and S. S. Ang, "Electromagnetic interference simulations for wide-bandgap power electronic modules," *IEEE J. Emerg. Sel. Topics Power Electron.*, vol. 4, no. 3, pp. 757–766, Sep. 2016.

[54] C. Yao *et al.*, "Comparison study of common-mode noise and thermal performance for lateral wire-bonded and vertically integrated high power diode modules," *IEEE Trans. Power Electron.*, vol. 33, no. 12, pp. 10572–10582, Dec. 2018.

[55] F. Zare, D. Kumar, M. Lungeanu, and A. Andreas, "Electromagnetic interference issues of power, electronics systems with wide band gap, semiconductor devices," in *Proc. IEEE Energy Convers. Congr. Expo. (ECCE)*, Montreal, QC, Canada, Sep. 2015, pp. 5946–5951.

[56] A. P. Camacho, V. Sala, H. Ghorbani, and J. L. R. Martinez, "A novel active gate driver for improving SiC MOSFET switching trajectory," *IEEE Trans. Ind. Electron.*, vol. 64, no. 11, pp. 9032–9042, Nov. 2017.

[57] H. C. P. Dymond *et al.*, "A 6.7-GHz active gate driver for GaN FETs to combat overshoot, ringing, and EMI," *IEEE Trans. Power Electron.*, vol. 33, no. 1, pp. 581–594, Jan. 2018.

[58] H. Huang, X. Yang, Y. Wen, and Z. Long, "A switching ringing suppression scheme of SiC MOSFET by active gate drive," in *Proc. IEEE 8th Int. Power Electron. Motion Control Conf. (IPEMC-ECCE Asia)*, Hefei, China, May 2016, pp. 285–291.

[59] M. Shahverdi, M. Mazzola, R. Schrader, A. Lemmon, and J. Gafford, "Active gate drive solutions for improving SiC JFET switching dynamics," in *Proc. 28th Annu. IEEE Appl. Power Electron. Conf. Expo. (APEC)*, Long Beach, CA, USA, Mar. 2013, pp. 2739–2743.

[60] S. U. Hasan and G. E. Town, "An aperiodic modulation method to mitigate electromagnetic interference in impedance source DC–DC converters," *IEEE Trans. Power Electron.*, vol. 33, no. 9, pp. 7601–7608, Sep. 2018.

[61] Y. Shi, Y. Zhang, L. Wang, and H. Li, "Reduction of EMI noise due to nonideal interleaving in a 100 kW SiC PV converter," *IEEE Trans. Power Electron.*, vol. 34, no. 1, pp. 13–19, Jan. 2019.

[62] Z. Liu, X. Huang, F. C. Lee, and Q. Li, "Package parasitic inductance extraction and simulation model development for the high-voltage cascode GaN HEMT," *IEEE Trans. Power Electron.*, vol. 29, no. 4, pp. 1977–1985, Apr. 2014.

[63] W. Zhang *et al.*, "A new package of high-voltage cascode gallium nitride device for megahertz operation," *IEEE Trans. Power Electron.*, vol. 31, no. 2, pp. 1344–1353, Feb. 2016.

[64] X. Huang, W. Du, F. C. Lee, Q. Li, and Z. Liu, "Avoiding Si MOSFET avalanche and achieving zero-voltage switching for cascode GaN devices," *IEEE Trans. Power Electron.*, vol. 31, no. 1, pp. 593–600, Jan. 2016.

[65] X. Huang, Q. Li, Z. Liu, and F. C. Lee, "Analytical loss model of high voltage GaN HEMT in cascode configuration," *IEEE Trans. Power Electron.*, vol. 29, no. 5, pp. 2208–2219, May 2014.

[66] X. Huang, W. Du, F. C. Lee, Q. Li, and W. Zhang, "Avoiding divergent oscillation of a cascode GaN device under high-current turn-off condition," *IEEE Trans. Power Electron.*, vol. 32, no. 1, pp. 593–601, Jan. 2017.

[67] E. Masuda *et al.*, "A study on wiring pattern design for intelligent SiC power module with PEEC method," in *Proc. Asia–Pacific Int. Symp. Electromagn. Compat. (APEMC)*, Seoul, South Korea, Jun. 2017, pp. 213–215.

[68] T. Ibuchi *et al.*, "A study on packaging design of SiC power module using near-field magnetic scanning techniques," in *Proc. IEEE Int. Workshop Integr. Power Packag. (IWIPP)*, Delft, The Netherlands, Apr. 2017, pp. 1–4.

[69] S. Li, L. M. Tolbert, F. Wang, and F. Z. Peng, "Stray inductance reduction of commutation loop in the P-cell and N-cell-based IGBT phase leg module," *IEEE Trans. Power Electron.*, vol. 29, no. 7, pp. 3616–3624, Jul. 2014.

[70] R. Wang, Z. Chen, D. Boroyevich, L. Jiang, Y. Yao, and K. Rajashekara, "A novel hybrid packaging structure for high-temperature SiC power modules," *IEEE Trans. Ind. Appl.*, vol. 49, no. 4, pp. 1609–1618, Jul. 2013.

[71] K. Wang, L. Wang, X. Yang, X. Zeng, W. Chen, and H. Li, "A multiloop method for minimization of parasitic inductance in GaN-based high-frequency DC–DC converter," *IEEE Trans. Power Electron.*, vol. 32, no. 6, pp. 4728–4740, Jun. 2017.

[72] K. Takao and S. Kyogoku, "Ultra low inductance power module for fast switching SiC power devices," in *Proc. IEEE 27th Int. Symp. Power Semiconductor Devices IC's (ISPSD)*, Hong Kong, May 2015, pp. 313–316.

[73] C. Chen, Y. Chen, Y. Li, Z. Huang, T. Liu, and Y. Kang, "An SiC-based half-bridge module with an improved hybrid packaging method for high power density applications," *IEEE Trans. Ind. Electron.*, vol. 64, no. 11, pp. 8980–8991, Nov. 2017.

[74] C. Chen, Z. Huang, L. Chen, Y. Tan, Y. Kang, and F. Luo, "Flexible PCB-based 3-D integrated SiC half-bridge power module with three-sided cooling using ultralow inductive hybrid packaging structure," *IEEE Trans. Power Electron.*, vol. 34, no. 6, pp. 5579–5593, Jun. 2019.

[75] F. Yang, Z. Liang, Z. J. Wang, and F. Wang, "Design of a low parasitic inductance SiC power module with double-sided cooling," in *Proc. IEEE Appl. Power Electron. Conf. Expo. (APEC)*, Tampa, FL, USA, Mar. 2017, pp. 3057–3062.

[76] F. Yang, Z. Wang, Z. Liang, and F. Wang, "Electrical performance advancement in SiC power module package design with kelvin drain connection and low parasitic inductance," *IEEE J. Emerg. Sel. Topics Power Electron.*, vol. 7, no. 1, pp. 84–98, Mar. 2019.

[77] A. S. Bahman, F. Blaabjerg, A. Dutta, and A. Mantooth, "Electrical parasitics and thermal modeling for optimized layout design of high power SiC modules," in *Proc. IEEE Appl. Power Electron. Conf. Expo. (APEC)*, Long Beach, CA, USA, Mar. 2016, pp. 3012–3019.

[78] Z. Liang, P. Ning, F. Wang, and L. Marlino, "Planar bond all: A new packaging technology for advanced automotive power modules," in *Proc. IEEE Energy Convers. Congr. Expo. (ECCE)*, Raleigh, NC, USA, Sep. 2012, pp. 438–443.

[79] N. Zhu, H. A. Mantooth, D. Xu, M. Chen, and M. D. Glover, "A solution to press-pack packaging of SiC MOSFETS," *IEEE Trans. Ind. Electron.*, vol. 64, no. 10, pp. 8224–8234, Oct. 2017.

[80] C. Fita, P.-O. Jeannin, P. Lefranc, E. Clavel, and J. Delaine, "A novel 3D structure for synchronous buck converter based on nitride Gallium transistors," in *Proc. IEEE Energy Convers. Congr. Expo. (ECCE)*, Milwaukee, WI, USA, Sep. 2016, pp. 1–7.

[81] G. Regnat, P.-O. Jeannin, D. Frey, J. Ewanchuk, S. V. Mollov, and J.-P. Ferrieux, "Optimized power modules for silicon carbide MOSFET," *IEEE Trans. Ind. Appl.*, vol. 54, no. 2, pp. 1634–1644, Mar./Apr. 2018.

[82] A. B. Jørgensen, S. Bęczkowski, C. Uhrenfeldt, N. H. Petersen, S. Jørgensen, and S. Munk-Nielsen, "A fast-switching integrated full-bridge power module based on GaN eHEMT devices," *IEEE Trans. Power Electron.*, vol. 34, no. 3, pp. 2494–2504, Mar. 2019.

[83] B. Zhang and S. Wang, "An overview of wide bandgap power semiconductor device packaging techniques for EMI reduction," in *Proc. IEEE Symp. Electromagn. Compat., Signal Integrity Power Integrity (EMC, SI PI)*, Long Beach, CA, USA, Jul./Aug. 2018, pp. 297–301.

[84] C. Chen, F. Luo, and Y. Kang, "A review of SiC power module packaging: Layout, material system and integration," *CPSS Trans. Power Electron. Appl.*, vol. 2, no. 3, pp. 170–186, Sep. 2017.

[85] L. Wang, Y. Shi, and H. Li, "Anti-EMI noise digital filter design for a 60-kW five-level SiC inverter without fiber isolation," *IEEE Trans. Power Electron.*, vol. 33, no. 1, pp. 13–17, Jan. 2018.

[86] H. Chen and D. Divan, "High speed switching issues of high power rated silicon-carbide devices and the mitigation methods," in *Proc. IEEE Energy Convers. Congr. Expo. (ECCE)*, Montreal, QC, Canada, Sep. 2015, pp. 2254–2260.

[87] E. Rondon-Pinilla, F. Morel, C. Vollaire, and J.-L. Schanen, "Modeling of a buck converter with a SiC JFET to predict EMC conducted emissions," *IEEE Trans. Power Electron.*, vol. 29, no. 5, pp. 2246–2260, May 2014.

[88] N. Zhang, S. Wang, and H. Zhao, "Develop parasitic inductance model for the planar busbar of an IGBT H bridge in a power inverter," *IEEE Trans. Power Electron.*, vol. 30, no. 12, pp. 6924–6933, Dec. 2015.

[89] S. Walder, X. Yuan, I. Laird, and J. J. O. Dalton, "Identification of the temporal source of frequency domain characteristics of SiC MOSFET based power converter waveforms," in *Proc. IEEE Energy Convers. Congr. Expo. (ECCE)*, Milwaukee, WI, USA, Sep. 2016, pp. 1–8.

[90] H. Li, S. Munk-Nielsen, S. Bęczkowski, and X. Wang, "SiC MOSFETs based split output half bridge inverter: Current commutation mechanism and efficiency analysis," in *Proc. IEEE Energy Convers. Congr. Expo. (ECCE)*, Pittsburgh, PA, USA, Sep. 2014, pp. 1581–1588.

[91] E. Velander *et al.*, "An ultralow loss inductorless dv/dt filter concept for medium-power voltage source motor drive converters with SiC devices," *IEEE Trans. Power Electron.*, vol. 33, no. 7, pp. 6072–6081, Jul. 2018.

[92] K. Yatsugi, K. Nomura, and Y. Hattori, "Analytical technique for designing an RC snubber circuit for ringing suppression in a phase-leg configuration," *IEEE Trans. Power Electron.*, vol. 33, no. 6, pp. 4736–4745, Jun. 2018.

[93] F. Zhao, Y. Li, Q. Tang, and L. Wang, "Analysis of oscillation in bridge structure based on GaN devices and ferrite bead suppression method," in *Proc. IEEE Energy Convers. Congr. Expo. (ECCE)*, Cincinnati, OH, USA, Oct. 2017, pp. 391–398.

[94] S. Wang, P. Kong, and F. C. Lee, "Common mode noise reduction for boost converters using general balance technique," *IEEE Trans. Power Electron.*, vol. 22, no. 4, pp. 1410–1416, Jul. 2007.

[95] K. Tsai, F. Qi, E. Davidson, and L. Xu, "Common mode EMI noise characterization and improvement for GaN switched-capacitor converter," in *Proc. IEEE Energy Convers. Congr. Expo.*, Denver, CO, USA, Sep. 2013, pp. 4159–4165.

[96] X. Liu, F. Costa, B. Revol, and, C. Gautier, "EMI investigation in a GaN HEMT power module," in *Proc. PCIM Eur., Int. Exhib. Conf. Power Electron., Intell. Motion, Renew. Energy Energy Manage.*, Nuremberg, Germany, May 2016, pp. 1–8.

[97] R. Robutel *et al.*, "Design and implementation of integrated common mode capacitors for SiC-JFET inverters," *IEEE Trans. Power Electron.*, vol. 29, no. 7, pp. 3625–3636, Jul. 2014.

[98] B. Sun, R. Burgos, X. Zhang, and D. Boroyevich, "Differential-mode EMI emission prediction of SiC-based power converters using a mixed-mode unterminated behavioral model," in *Proc. IEEE Energy Convers. Congr. Expo. (ECCE)*, Montreal, QC, Canada, Sep. 2015, pp. 4367–4374.

[99] P. Bogónez-Franco and J. B. Sendra, "EMI comparison between Si and SiC technology in a boost converter," in *Proc. Int. Symp. Electromagn. Compat.-EMC EUROPE*, Rome, Italy, Sep. 2012, pp. 1–4.

[100] Y. Yang, Z. Liu, F. C. Lee, and Q. Li, "Analysis and filter design of differential mode EMI noise for GaN-based interleaved MHz critical mode PFC converter," in *Proc. IEEE Energy Convers. Congr. Expo. (ECCE)*, Pittsburgh, PA, USA, Sep. 2014, pp. 4784–4789.

[101] J. Sun, W. Chen, and X. Yang, "EMI prediction and filter design for MHz GaN based LLC half-bridge converter," in *Proc. IEEE 8th Int. Power Electron. Motion Control Conf. (IPEMC-ECCE Asia)*, Hefei, China, May 2016, pp. 297–304.

[102] X. Huang, J. Feng, F. C. Lee, Q. Li, and Y. Yang, "Conducted EMI analysis and filter design for MHz active clamp flyback front-end converter," in *Proc. IEEE Appl. Power Electron. Conf. Expo. (APEC)*, Long Beach, CA, USA, Mar. 2016, pp. 1534–1540.

[103] S. Narasimhan, S. Tewari, E. Severson, R. Baranwal, and N. Mohan, "Mitigation of common-mode noise in wide band gap device based motor drives," in *Proc. IEEE Appl. Power Electron. Conf. Expo. (APEC)*, Long Beach, CA, USA, Mar. 2016, pp. 2043–2050.

[104] S. Ohn *et al.*, "Three-terminal common-mode EMI model for EMI generation, propagation, and mitigation in a full-SiC three-phase UPS module," *IEEE Trans. Power Electron.*, vol. 34, no. 9, pp. 8599–8612, Sep. 2019.

[105] D. Hamza, M. Qiu, and P. K. Jain, "Application and stability analysis of a novel digital active EMI filter used in a grid-tied PV microinverter module," *IEEE Trans. Power Electron.*, vol. 28, no. 6, pp. 2867–2874, Jun. 2013.

[106] J. Ji, W. Chen, X. Yang, and J. Lu, "Delay and decoupling analysis of a digital active EMI filter used in arc welding inverter," *IEEE Trans. Power Electron.*, vol. 33, no. 8, pp. 6710–6722, Aug. 2018.

[107] B. I. Incau, I. Trintis, and S. Munk-Nielsen, "Switching speed limitations of high power IGBT modules," in *Proc. 17th Eur. Conf. Power Electron. Appl. (EPE'15 ECCE-Eur.)*, Geneva, Switzerland, Sep. 2015, pp. 1–8.

[108] K. Umetani, R. Matsumoto, and E. Hiraki, "Prevention of oscillatory false triggering of GaN-FETs by balancing gate-drain capacitance and common-source inductance," *IEEE Trans. Ind. Appl.*, vol. 55, no. 1, pp. 610–619, Jan./Feb. 2019.

[109] A. Lemmon, M. Mazzola, J. Gafford, and C. Parker, "Instability in half-bridge circuits switched with wide band-gap transistors," *IEEE Trans. Power Electron.*, vol. 29, no. 5, pp. 2380–2392, May 2014.

[110] M. K. Kazimierczuk, *RF Power Amplifiers*. New York, NY, USA: Wiley, 2015, pp. 543–545.

[111] D.-P. Sadik, K. Kostov, J. Colmenares, F. Giezendanner, P. Ranstad, and H.-P. Nee, "Analysis of parasitic elements of SiC power modules with special emphasis on reliability issues," *IEEE J. Emerg. Sel. Topics Power Electron.*, vol. 4, no. 3, pp. 988–995, Sep. 2016.

[112] H. Li, S. Munk-Nielsen, X. Wang, S. Bęczkowski, S. R. Jones, and X. Dai, "Effects of auxiliary-source connections in multichip power module," *IEEE Trans. Power Electron.*, vol. 32, no. 10, pp. 7816–7823, Oct. 2017.

[113] Z. Zhang, F. Wang, L. M. Tolbert, and B. J. Blalock, "Active gate driver for crosstalk suppression of SiC devices in a phase-leg configuration," *IEEE Trans. Power Electron.*, vol. 29, no. 4, pp. 1986–1997, Apr. 2014.

[114] Y. Li, M. Liang, J. Chen, T. Q. Zheng, and H. Guo, "A low gate turn-off impedance driver for suppressing crosstalk of SiC MOSFET based on different discrete packages," *IEEE J. Emerg. Sel. Topics Power Electron.*, vol. 7, no. 1, pp. 353–365, Mar. 2019.

[115] B. Zhang, S. Xie, J. Xu, Q. Qian, Z. Zhang, and K. Xu, "A magnetic coupling based gate driver for crosstalk suppression of SiC MOSFETs," *IEEE Trans. Ind. Electron.*, vol. 64, no. 11, pp. 9052–9063, Nov. 2017.

[116] J. Wang and H. S.-H. Chung, "A novel RCD level shifter for elimination of spurious turn-on in the bridge-leg configuration," *IEEE Trans. Power Electron.*, vol. 30, no. 2, pp. 976–984, Feb. 2015.

[117] F. Gao, Q. Zhou, P. Wang, and C. Zhang, "A gate driver of SiC MOSFET for suppressing the negative voltage spikes in a bridge circuit," *IEEE Trans. Power Electron.*, vol. 33, no. 3, pp. 2339–2353, Mar. 2018.

[118] T. Zhu, F. Zhuo, F. Zhao, F. Wang, and T. Zhao, "Quantitative model-based false turn-on evaluation and suppression for cascode GaN devices in half-bridge applications," *IEEE Trans. Power Electron.*, vol. 34, no. 10, pp. 10166–10179, Oct. 2019.

[119] Z. Liu, "Characterization and failure mode analysis of cascode GaN HEMT," Ph.D. dissertation, Elect. Eng., Virginia Tech., Blacksburg, VA, USA, 2014.

[120] Z. Dong, X. Wu, and K. Sheng, "Suppressing methods of parasitic capacitance caused interference in a SiC MOSFET integrated power module," *IEEE J. Emerg. Sel. Topics Power Electron.*, vol. 7, no. 2, pp. 745–752, Jun. 2019.
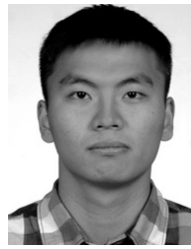
Boyi Zhang (S'17) received the B.S. degree in electrical engineering from the Harbin Institute of Technology, Harbin, China, in 2015, and the M.S. degree in electrical and computer engineering from the University of Florida, Gainesville, FL, USA, in 2017, where he is currently pursuing the Ph.D. degree with the Power Electronics and Electrical Power Research Laboratory.

He has authored or coauthored several IEEE conference and transaction articles. His research interests include electromagnetic interference, wide-bandgap power device packaging, and magnetic components.

Mr. Zhang received the Best Student Presentation Awards at the Applied Power Electronics Conference (APEC) in 2017 and 2019.

Shuo Wang (S'03–M'06–SM'07–F'19) received the Ph.D. degree in electrical engineering from Virginia Tech, Blacksburg, VA, USA, in 2005.

He is currently a Full Professor with the Department of Electrical and Computer Engineering, University of Florida, Gainesville, FL, USA. He has published more than 180 IEEE journal and conference articles. He holds around 30 pending/issued U.S./international patents.

Dr. Wang received the Best Transaction Paper Award from the IEEE Power Electronics Society in 2006 and two William M. Portnoy Awards for the articles published in the IEEE Industry Applications Society in 2004 and 2012, respectively. In 2012, he received the prestigious National Science Foundation CAREER Award. He is also the Technical Program Co-Chair of the IEEE 2014 International Electric Vehicle Conference. He is also an Associate Editor of the IEEE TRANSACTIONS ON INDUSTRY APPLICATIONS.